This document is downloaded from the
Digital Open Access Repository of VTT

| | |
|---|---|
| Title | Aluminum oxide from trimethylaluminum and water by atomic layer deposition: The temperature dependence of residual stress, elastic modulus, hardness and adhesion |
| Author(s) | Ylivaara, O.; Liu, X.; Kilpi, L.; Lyytinen, J.; Schneider, D.; Laitinen, M.; Julin, J.; Ali, S.; Sintonen, S.; Berdova, M.; Haimi, E.; Sajavaara, T.; Ronkainen, H.; Lipsanen, H.; Koskinen, J.; Hannula, S.-P.; Puurunen, R. |
| Citation | Thin Solid Films. Elsevier . Vol. 52 (2014), Pages 124 - 135 |
| Date | 2014 |
| URL | http://dx.doi.org/10.1016/j.tsf.2013.11.112 |
| Rights | © 2016. This manuscript version is made available under the CC-BY-NC-ND 4.0 license http://creativecommons.org/licenses/by-nc-nd/4.0/ |

Self archived 8th December 2016

| | |
|---|---|
| VTT<br>http://www.vtt.fi<br>P.O. box 1000<br>FI-02044 VTT<br>Finland | By using VTT Digital Open Access Repository you are bound by the following Terms & Conditions.<br><br>I have read and I understand the following statement:<br><br>This document is protected by copyright and other intellectual property rights, and duplication or sale of all or part of any of this document is not permitted, except duplication for research use or educational purposes in electronic or print form. You must obtain permission for any other use. Electronic or print copies may not be offered for sale. |

*Manuscript final version
Click here to view linked References

# Aluminum oxide from trimethylaluminum and water by atomic layer deposition: the temperature dependence of residual stress, elastic modulus, hardness and adhesion

Running title: ALD $Al_2O_3$ stress, elastic modulus, hardness and adhesion

Running Authors: Ylivaara et al.

Oili M. E. Ylivaara*)

VTT Technical Research Centre of Finland, P. O. Box 1000, FI-02044 Espoo, Finland

Xuwen Liu

Aalto University School of Chemical Technology, Department of Materials Science and Engineering, P. O. Box 16200, FI-00076 Aalto, Finland

Lauri Kilpi

VTT Technical Research Centre of Finland, P. O. Box 1000, FI-02044 Espoo, Finland

Jussi Lyytinen

Aalto University School of Chemical Technology, Department of Materials Science and Engineering, P. O. Box 16200, FI-00076 Aalto, Finland

Dieter Schneider

Fraunhofer IWS Dresden, Winterbergstrasse 28, 01277 Dresden, Germany

Mikko Laitinen

University of Jyväskylä, Department of Physics, P. O. Box 35, FI-40014 Jyväskylä, Finland

Jaakko Julin

University of Jyväskylä, Department of Physics, P. O. Box 35, FI-40014 Jyväskylä, Finland

Saima Ali

Aalto University School of Electrical Engineering, Department of Micro- and Nanosciences, P. O. Box 13500, FI-00076 Aalto, Finland

Sakari Sintonen

Aalto University School of Electrical Engineering, Department of Micro- and Nanosciences, P. O. Box 13500, FI-00076 Aalto, Finland

Maria Berdova

Aalto University, Department of Materials Science and Engineering and Micronova Nanofabrication Center, P. O. Box 13500, FI-00076 Aalto, Finland

Eero Haimi

Aalto University School of Chemical Technology, Department of Materials Science and Engineering, P. O. Box 16200, FI-00076 Aalto, Finland

Timo Sajavaara

University of Jyväskylä, Department of Physics, P. O. Box 35, FI-40014 Jyväskylä, Finland

Helena Ronkainen

VTT Technical Research Centre of Finland, P. O. Box 1000, FI-02044 Espoo, Finland

Harri Lipsanen

Aalto University School of Electrical Engineering, Department of Micro- and Nanosciences, P. O. Box 13500, FI-00076 Aalto, Finland

Jari Koskinen

Aalto University School of Chemical Technology, Department of Materials Science and Engineering, P. O. Box 16200, FI-00076 Aalto, Finland

Simo-Pekka Hannula

Aalto University School of Chemical Technology, Department of Materials Science and Engineering, P. O. Box 16200, FI-00076 Aalto, Finland

Riikka L. Puurunen

VTT Technical Research Centre of Finland, P. O. Box 1000, FI-02044 Espoo, Finland

OMEY designed the experiments together with RLP and fabricated samples in the Picosun's reactor. OMEY made the residual stress measurements and analysis under the supervision of RLP. XWL and EH made nanoindentation measurements under supervision of SPH. LK made the microscratching under supervision of HR. XWL and JL made scanning nanowear under supervision of JK. DS made LSAW measurements. ML and JJ made TOF-ERDA measurements under supervision of TS. SA and SS made XRR measurements and analysis under supervision of HL. MB made the growth with BENEQ's ALD reactor. OMEY interpreted the data and wrote the literature review under supervision of RLP. RLP was the main author responsible of the ALD growth discussion. Authors doing the measurements discussed the results and implications and commented on the manuscript by OMEY at all stages.

[*)]Electronic mail: oili.ylivaara@vtt.fi

Use of atomic layer deposition (ALD) in microelectromechanical systems (MEMS) has increased as ALD enables conformal growth on 3-dimensional structures at relatively low temperatures. For MEMS device design and fabrication, the understanding of stress and mechanical properties such as elastic modulus, hardness and adhesion of thin film is crucial. In this work a comprehensive characterization of the stress, elastic modulus, hardness and adhesion of ALD aluminum oxide ($Al_2O_3$)

films grown at 110 – 300 °C from trimethylaluminum and water is presented. Film stress was analyzed by wafer curvature measurements, elastic modulus by nanoindentation and surface-acoustic wave measurements, hardness by nanoindentation and adhesion by microscratch test and scanning nanowear. The films were also analyzed by ellipsometry, optical reflectometry, x-ray reflectivity and time-of-flight elastic recoil detection for refractive index, thickness, density and impurities. The ALD $Al_2O_3$ films were under tensile stress in the scale of hundreds of MPa. The magnitude of the stress decreased strongly with increasing ALD temperature. The stress was stable during storage in air. Elastic modulus and hardness of ALD $Al_2O_3$ saturated to a fairly constant value for growth at 150 to 300°C, while ALD at 110°C gave softer films with lower modulus. ALD $Al_2O_3$ films adhered strongly on cleaned silicon with $SiO_x$ termination.

## Keywords

Atomic layer deposition, ALD, residual stress, elastic modulus, hardness, adhesion, $Al_2O_3$, aluminum oxide

# I. INTRODUCTION

Atomic layer deposition (ALD) is based on the sequential use of self-limiting surface reactions [1][2][3]. The self-limiting nature of ALD enables growth of a film with a fraction of monolayer thicknesses [1][2]. Besides the precise thickness control, major advantages of ALD are the low growth temperature compared to chemical vapor deposition (CVD), uniformity [4] and conformality [5] of the film over high aspect ratio structures, and the ability to deposit functional ultrathin pinhole free films [6]. These properties and the versatile selection of precursors [1,7,8] has made ALD an attractive growth method in microelectromechanical systems (MEMS) devices

where membranes and cavities with high aspect ratio 3D structures are often present, and highly conformal films with tailored optical, mechanical or electrical properties are desired [9]. The use of ALD has been demonstrated in different applications, such as in RF-MEMS capacitive switches with $Al_2O_3/ZnO$ nanolaminate [10] or $HfO_2$ [11] as a dielectric layer, in Fabry-Perot interferometers with $Al_2O_3/TiO_2$ Bragg mirror stacks [12,13], in micromachined resonators with $Al_2O_3$ as a structural layer [14], as well as in a buried layer of $Al_2O_3$ and $TiO_2$ in wafer bonding [15] or as a protective coating [16].

Deposited thin film has residual stress, which can be either tensile or compressive. The magnitude and distribution of the stress depends on the deposition method (CVD, sputtering, ALD etc.) and process conditions (temperature, pressure, etc.). The thermal stress component originates from thermal expansion mismatch between the substrate and the deposited thin film; films are often deposited above room temperature and temperature change causes volume change [17]. Growth-induced stress in polycrystalline film is caused by phase transformations and composition changes for example due to film densification [18][19]. For amorphous films, residual stress is often observed but its origin is not generally understood. Small tensile residual stress is often preferred in MEMS, as this keeps the membranes flat. Tensile residual stress increases the bending stiffness while compressive stress reduces it and can lead to buckling [20]. $Al_2O_3$ is amongst the ALD material most used for MEMS applications. Stress behavior of ALD $Al_2O_3$ made from $AlMe_3$ and $H_2O$ has been studied [21][22][23][24] and a trend of decreasing magnitude of tensile residual stress with increasing growth temperature has been detected. In plasma-assisted ALD of $Al_2O_3$ impact of ions can result in compressive stress, which can be tuned even to tensile with substrate biasing [25].

Elastic modulus is an intrinsic material property and fundamentally related to atomic bonding. Therefore, elastic modulus does not depend on the shape or dimensions of the material; it characterizes the material stiffness and is one of the most used material constants in MEMS design [26]. Hardness, on the other hand, is a measure of the ability of a solid material to resist permanent deformation [27] and thus is an engineering property with its scale depending on measuring system. Since hardness signifies the plastic response of a solid material under external loads, it can be a good indicator for material resistance to wear, scratch and deformation failure. The elastic modulus and hardness of ALD $Al_2O_3$ has been measured by nanoindentation [10][22][28][24][29] and modulus by extraction from oscillator resonance frequency [30]. Both the modulus and hardness have been reported to increase with increasing growth temperature [10][29].

Interfacial phenomenon such as adhesion has great influence on the performance and reliability of the MEMS devices [31]. Adhesion failure is often the primary failure mechanism of the film, limiting its applicability and lifetime. The thin film adhesion is often tested using a Scotch tape method where a pressure sensitive tape is pressed on to the film and rapidly stripped [32]. This method gives qualitative “go—no go” information; if a film fails; adhesion is generally too poor for practical applications. For fine-tuning processes for better adhesion, more accurate measurement methods are needed. The scratch adhesion testing has been extensively used to assess the adhesion strength of coated surfaces [33][34][35]. The adhesion of ALD $Al_2O_3$ on Si, $SiO_2$, and polymer substrates has been recently studied by scratch testing for films made from $Me_3Al$ and $H_2O$ at 200 °C [36] and $Me_3Al$ and $O_3$ at 60 – 65 °C [37]. The adhesion was found to be the highest on $SiO_2$ [36]. Additionally, on the basis of four-point bending analysis, increased amount of ALD $Al_2O_3$ cycles in an

ALD $Al_2O_3$–Ru laminate grown at 225 °C has been observed to promote adhesion [38]. The adhesion energy furthermore correlated with the amount of interfacial Al–O–Si bonds formed [38].

The ALD process to deposit $Al_2O_3$ from $Me_3Al$ and $H_2O$ is perhaps the most studied ALD process, which—due to its practically ideal ALD behavior—has been adopted as a model system for understanding ALD growth and chemistry in general [1][3][8][39]. Second only to the choice of the ALD reactants, the ALD temperature is the most important parameter influencing the film properties [8]. Despite the fact that several studies have reported on the mechanical properties of ALD $Al_2O_3$ films, a systematic study reporting on the mechanical properties as a function of ALD temperature has been missing. Consequently, the goal of this work was to fill the gap in the existing knowledge, by creating a consistent set of data—as a function of the ALD temperature as well as other relevant process parameters, including the reactor type—on the film stress, elastic modulus, hardness and adhesion of ALD $Al_2O_3$ films made from $Me_3Al$ and $H_2O$ on silicon. To support the measurements, extensive physicochemical characterization of the films was carried out. The results were compared with existing literature, and conclusions were drawn and, if needed, updated, on the trends in the mechanical properties of ALD $Al_2O_3$ films as a function of the ALD temperature.

# II. EXPERIMENTAL DETAILS

## A. Sample preparation

ALD films were grown on 150 mm p-type (100) silicon wafers in a ISO 4 cleanroom. Double side polished (DSP) wafers with thickness of 380 ± 5 µm were used for stress measurements, and single side polished (SSP) wafers with thickness of

675 ± 15 μm for other characterization. The wafers were wet cleaned before the film growth using RCA -cleaning sequence (SC-1, diluted HF and SC-2) followed by deionized water rinses between the cleaning baths and spin-drying at the end of cleaning cycle. SC-1 is a mixture of deionized water, ammonia and hydrogen peroxide ($H_2O:NH_3:H_2O_2$ 5:1:1) where wafers were for 10 minutes at 65 °C with megasonic on. Hereupon the wafers were dipped in HF ($H_2O$:HF(50%) 50:1) for 30 seconds at room temperature and finally cleaned in SC-2, mixture of deionized water, ammonium hydroxide and hydrogen peroxide ($H_2O:NH_4OH:H_2O_2$ 5:1:1), for 10 minutes at 65 °C. After cleaning, the wafers were covered with a thin, about 1 - 2 nm thick chemical oxide ($SiO_x$).

Films were grown in a Picosun™ R-150 top-flow ALD reactor. The intermediate space pressure was about 7 hPa and there was a constant 200 sccm nitrogen (purity > 99.999%) flow through reactant lines. Trimethylaluminum ($Me_3Al$) from SAFC Hitech with electronic grade and deionized water ($H_2O$) were used as the precursors for the $Al_2O_3$ film. $Me_3Al$ bubbler was cooled with Peltier element to about 17 °C. Water was used at room temperature. The precursor dose and purge times were 0.1 and 4.0 s, respectively. For some samples grown at 300 °C, a faster, optimized recipe was used, where the dose and purge sequence for precursors was (0.1-1.0-0.1-1.0) s. The temperature range for film growth was from 110 to 300 °C. The number of growth cycles was varied from 10 to 6000 corresponding film thicknesses of roughly 10 to 600 nm. For stress measurements, films were grown on the front side of the DSP wafers. Growth to the backside of the wafer was prevented by protecting the backside with 150 mm SSP wafer, rough side against the backside. Despite the backside protection, a visible 1 to 5 mm edge ring was grown on the backside of the wafers.

For comparison of the film stress, some films were grown in a Beneq TFS-500 cross-flow ALD reactor. Temperatures were 120, 150, 200, 250 and 300 °C, and the cycle numbers 1050, 1025, 950, 900 and 900, respectively, targeted to give film thickness of 100 nm. The pulsing sequence was kept constant (0.25-0.75-0.20-0.75) s. Actual film thicknesses were 103.5, 107.1, 105.5, 101.0 and 93.3 nm, and the standard deviations based on 49-point reflectometer measurements were 2.3, 0.4, 0.5, 1.0 and 0.3 nm, for the films grown at 120, 150, 200, 250 and 300 °C, respectively. Growth was one sided, with a visible 1 to 5 mm edge ring grown on the backside of the wafers.

## B. Characterization

### 1. Physicochemical characterization

Film thicknesses were measured with FilmTek 2000M spectroscopic reflectometry in a 49-point automated measurement. Dispersion of refractive index for the $Al_2O_3$ recipe was measured by equipment manufacturer SCI FilmTek for a film grown at 300 °C in 5000 cycles. For some wafers, thickness and refractive index were measured with a Plasmos spectroscopic ellipsometer using 633 nm wavelength (HeNe laser) and 70° incident angle with floating refractive index.

The film composition and impurities were analyzed with time-of-flight elastic recoil detection analysis (TOF-ERDA). The self-built equipment uses 10.2 MeV $^{35}Cl$ and 11.9 MeV $^{63}Cu$ ions from a 1.7 MV Pelletron accelerator [40]. The major advantage of TOF-ERDA is that it enables quantitative detection and depth profiling of hydrogen and other light elements in addition to the heavy ones.

Density was measured with X-ray reflectivity (XRR). The measurement instrument was a Philips X'Pert Pro diffractometer using Cu Kα wavelength with

40 kV and 40 mA voltage and current, respectively. The XRR analysis generated information also on film thickness and surface roughness. The XRR results are based on the simulations and thus the accuracy in each case is case dependent. The accuracy values are in range of ±0.05 g/cm$^3$ for the density, ±0.2 – 2 nm for the film thickness and ±0.3 nm for the roughness.

## 2. *Wafer curvature measurement*

Residual stress was determined by wafer curvature method. Curvature was measured before and after film growth with a Veeco DEKTAK V200-Si stylus profilometer. Wafers were scanned parallel and perpendicular to the wafer flat using a 120 mm scan length. Wafer curvature was analyzed through the scan area and the stress was determined with Veeco's Stress Measurement Analysis software that uses Stoney's equation [41]

$$\sigma_f = -\frac{E_s}{6(1-\upsilon_s)}\frac{t_s^2}{t_f}\left(\frac{1}{R_1}-\frac{1}{R_0}\right), \qquad (1)$$

where $\sigma_f$ is the thin film stress [Pa] (negative for compressive stress), $E_s$ is the elastic modulus of the substrate [Pa], $\upsilon_s$ the Poisson's ratio of the substrate, $R_0$ and $R_1$ are the radius of curvature before and after the film growth [m], respectively, and $t_s$ and $t_f$ are the thicknesses of the substrate and the film [m]. $E_s/(1-\upsilon_s)$ is a biaxial modulus having a constant value of $1.805 \times 10^{11}$ Pa for (100) Si [42].

Reliability of the wafer curvature measurement was evaluated with repeated measurements. Three persons measured three wafers having 100 nm $Al_2O_3$ layer grown at 300 °C in 1000 cycles (0.1-1.0-0.1-1.0) s. Measurements were repeated three times before and after ALD. Stresses were calculated and average and standard deviation were determined on the basis of 27 measurements. Average residual stress

of 214 ± 18 MPa (tensile) was measured giving a relative standard deviation of 8 % for 120 mm scan of 100 nm $Al_2O_3$ grown at 300 °C in 1000 cycles [pulse sequence (0.1-1.0-0.1-1.0) s]. Maximum measurement error was approximated using total differential of Equation 1. As the radius of curvature, *R* can be expressed as $R = l^2/8h$ [43], the Equation 1 can be presented as follows

$$\sigma_f = -\frac{E_s}{6(1-\upsilon_s)}\frac{t_s^2}{t_f}\left(\frac{8h_1}{l^2}-\frac{8h_0}{l^2}\right) = -\frac{E_s}{6(1-\upsilon)}\frac{t_s^2}{t_f}\frac{8}{l^2}(h_1 - h_0), \quad (2)$$

where $h_0$ is the initial wafer deflection [m], $h_1$ is the wafer deflection after the film growth [m] and $l$ is the scan length [m]. The maximum measurement error was determined using total differential of $\Delta\sigma$.

$$\Delta\sigma = \left|\frac{\partial\sigma}{\partial t_s}\right|\Delta t_s + \left|\frac{\partial\sigma}{\partial t_f}\right|\Delta t_f + \left|\frac{\partial\sigma}{\partial h_1}\right|\Delta h_1 + \left|\frac{\partial\sigma}{\partial h_0}\right|\Delta h_0, \quad (3)$$

where $\Delta h_0$ and $\Delta h_1$ are the measurement error in wafer deflection before and after the film growth, while $\Delta t_f$ and $\Delta t_s$ are the error in film and substrate thickness. Numerical values for the Equation 3 were obtained from repeated measurements made for 100 nm $Al_2O_3$ grown at 300 °C in 1000 cycles on 380 μm wafers. Error values used in calculation were $\Delta h_0 = 1200nm$, $\Delta h_1 = 1200nm$, $\Delta t_f = 1.3nm$ and $\Delta t_s = 5\mu m$. Maximum measurement error of 65 MPa was calculated for the 100 nm film. This was 30% of average residual stress value, 214 MPa. The maximum measurement error is larger for thinner films.

The effect of the backside edge ring on the stress was examined on wafer having 600 nm thick $Al_2O_3$ layer grown at 300 °C in 6000 cycles (0.1-1.0-0.1-1.0) s. The front side of the wafer was protected with photoresist and the backside was etched in buffered hydrofluoric acid (BHF). Residual stress was 4 % higher after

backside ring removal. The influence of backside growth was considered to be within the experimental accuracy.

## 3. Nanoindentation

Nanoindentation measurements were carried out with a Hysitron TriboIndenter® TI-900 nano-mechanical testing system. Measurements were done in a semi-clean room with constant laminar airflow to minimize the possible thermal drift during the measurements. Indentations were performed under load-control mode with the loading, holding at peak-load and unloading segment times of 10, 5 and 5 seconds, respectively.

A cube-corner indenter with a 90° total induced angle and a tip radius under 40 nm was used in the study. The purpose of using a sharp tip was to trigger plastic deformation at shallow indents, less than 10% of the film thickness, in order to measure the film hardness with minimal substrate effects.

The mechanical properties of the indented material were extracted from a series of load and depth data using the Oliver and Pharr method [44], where the elastic modulus of the film, $E_f$ and the diamond tip, $E_i$ are related to the contact modulus, $E^*$, through the following equation

$$\frac{1}{E^*} = \frac{1-\upsilon_i^2}{E_i} + \frac{1-\upsilon_f^2}{E_f}, \qquad (4)$$

where $\upsilon_i$ and $\upsilon_f$ are the Poisson´s ratio for the diamond tip and grown film (or the Si reference), respectively. For diamond tip 1140 GPa and 0.07 were used for $E_i$ and $\upsilon_i$, respectively. Poisson´s ratio of $\upsilon_f = 0.24$ [24] was used for the $Al_2O_3$ films and 0.25 for silicon (Ref. [45] gives a wide range of Poisson's ratios for Si, 0.048 - 0.403, due

to the anisotropic nature of Si; our average value should be reasonable considering the orientation of our Si). The hardness of the film is defined as the maximum indentation load divided by the contact area corresponding to the load [46]

$$H = \frac{P_{max}}{A} . \qquad (5)$$

The instrument stability and indentation repeatability were monitored by performing a series of 16 indents into a piece of silicon wafer over a period of time with the peak load varying from 5 to 500 μN. The silicon reference sample was taken from the same wafer batch that was used as the substrate for the $Al_2O_3$ films. The indenter conditions (tip rounding) were also checked throughout the measurement by indenting on the standard fused quartz to see the need of the tip area function for recalibration.

## 4. Laser-generated surface acoustic wave measurement

For comparison to the nanoindentation technique, laser-generated surface acoustic wave (LSAW) measurements [47] were performed on ALD $Al_2O_3$ films grown at 300 °C on silicon. The technique uses short pulses of a nitrogen laser focused into a line to create wide-band surface acoustic waves detected by piezoelectric transducer. The device measures the dispersion spectrum. The material parameters of the film were calculated by fitting a dispersion curve deduced from a theory of surface acoustic wave dispersion. The spot of the measurement was 3 × 10 mm. Three measurements per sample were performed along (110) direction of the (100) silicon wafer. For $Al_2O_3$ grown at 300 °C Poisson's ratio of 0.24 [24] and XRR measured average density of 3.1 g/cm$^3$ were used. And for silicon density of 2.33 g/cm$^3$, and elastic stiffness values of $C_{12}$ = 63.5 GPa and $C_{44}$ = 79.6 GPa. For all the samples, stiffness of $C_{11}$ of 165.5 ± 0.2 GPa was fitted by extrapolating the

dispersion curve to 0 MHz frequency. In comparison to the nanoindentation, the LSAW technique has a higher precision, but a poorer lateral resolution. In case of porous materials nanoindentation and LSAW may give systematically different results but for isotropic compact films and bulk materials, both methods yield the same values.

## *5. Microscratch testing*

Adhesion performance of about 300 nm ALD $Al_2O_3$ films grown at 110 - 300 °C on RCA-cleaned silicon was evaluated with microscratch testing [35] using CSM Micro combi tester. The experiments were carried out in a controlled temperature and humidity, 22 ± 1 °C and 50 ± 5 %, respectively. Scratches were generated with a Rockwell C diamond tip with the radius of 20 µm and with continuously increasing normal force, from 0.05 to 1.0 N. The scratch length was 3 mm and scratching speed 10 mm/min. Three scratches were done for each sample while scratches being 0.5 mm apart from each other. The normal force, tangential force, friction coefficient, acoustic emission and penetration depth were monitored during testing.

For the measurements the ALD $Al_2O_3$ coated silicon samples were glued with an adhesive (Henkel's Loctite 401) onto aluminum (Al 6082) discs (thickness 10 mm and diameter 40 mm), which were attached to the tester. After the scratch testing a panorama image was taken and the scratch channel was investigated with optical microscopy to determine the critical loads. Generally the critical loads for surface coatings are defined according to the crack generation and delamination criteria as described in the C1624-05 standard [48]. However, for the thin ALD films deposited on Si wafers, these criteria were not applicable. Therefore, in this work, a criterium

for coating/substrate system behavior in scratch testing has been developed. The observed continuous Si breakage point was determined as the first critical load ($L_{CSi}$) and the observed ALD coating adhesion failure was the second critical load ($L_{CALD}$). After scratching selected samples were also analyzed using the scanning electron microscope (SEM) with an energy-dispersive X-ray spectrometry (EDS);
FEI XL 30 ESEM. EDS analysis was carried out at 15 kV accelerating voltage.

### *6. Scanning nanowear*

Scanning nanowear was carried out with the nanoindentation instrument, presented earlier, on a 100 nm thick ALD $Al_2O_3$ film grown at 300 °C. At first, a 5 x 5 µm area on the film surface was selected and the area was scanned at a set-load of 1.5 µN. Then, nanowear was performed in a 3 x 3 µm area within the scanned region in a single path with stepwise increased set-loads of 10, 20, 30 and 40 µN. The idea was to establish the knowledge on the material removal behavior to gain better understanding on the failure mechanism of the film in wear and to observe possible adhesion failure and delamination of the film. Finally, nanowear at a 50 µN set-load and in a 3 x 3 µm area was performed in a single path, aimed to observe film adhesion behavior and to remove the film and reveal the Si substrate. The frequency in the scanning wear was 1 Hz and the tip velocity was 6 µm/s. After the nanowear, the worn region was characterized using SEM.

# III. RESULTS

## *A. Thin film characterization*

Thickness of ALD $Al_2O_3$ increased linearly as a function of growth cycles. In Figure 1a, the thickness of $Al_2O_3$ film grown at 300 °C [pulse sequence of (0.1-1.0-0.1-1.0) s] is presented as a function of ALD cycles. A fitted line intersects *y*-axis at

about 1 nm, revealing the presence of the $SiO_x$ layer on RCA-cleaned Si. The film thickness divided by the number of ALD cycles, thickness per cycle, first increased as a function of temperature, went through a maximum, and thereafter decreased with increasing ALD temperature (Figure 1b). The thickness per cycle trend with temperature was similar as reported in earlier studies [49][50][51][52][53][54][55].

The effect of a repeated number of precursor doses was studied with 100 nm $Al_2O_3$ film grown at 110 and 300 °C. The Picosun[TM] R-150 ALD reactor enables the separate adjustment of the precursor pulse and purge times and the number of repeats for precursor doses. $Me_3Al$ and $H_2O$ doses were increased about fivefold by repeated pulses. At 110 °C the film thickness increased as a result of multiplied precursor pulses (read increased dose) from 94 ± 3 to 152 ± 3 nm. This indicates that the ALD growth was not fully saturated; change in thickness per cycles with increased precursor dose was seen in Figure 1B. At 300 °C multiplication of pulses was tested using two recipes with two different pulse sequences (0.1-1.0-0.1-1.0) and (0.1-4.0-0.1-4.0) s. In first case the film thickness increased from 95 ± 1 to 108 ± 1 nm with increased dosing and in latter case the film thickness increased from 100 ± 1 to 111 ± 1 nm. The smaller increase of film thickness as compared to the growth made at 110 °C indicates that the ALD growth was closer to saturation at 300 °C than it was at 110 °C.

$Al_2O_3$ films were characterized in an ALD temperature range of 110 to 300 °C. Spectroscopic reflectometer, ellipsometer and XRR thickness measurements were in close agreement, presented in Table 1. At highest growth temperature, at 300 °C, the measured standard deviation for thickness (49 measurement points) was smallest, around 1%, while the uniformity was acceptable also at the lowest temperatures (<3%). Refractive index, measured for

about 100 nm films, increased slightly with increasing ALD temperature, in accordance with earlier publications [52][55]. For the film grown at 110 °C the refractive index was 1.62 and at 300 °C it was increased to 1.66. The XRR film density increased almost linearly with increasing ALD temperature from 2.85 to 3.10 g/cm$^3$ for films grown at 110 to 250 °C. At 250 °C and higher temperatures the density saturated to 3.10 g/cm$^3$, in line with literature [52][55]. Refractive index correlated linearly with density ($R^2$=0.973). Constant film densities were measured with increasing film thickness, within the measurement accuracy of the XRR. Roughness's measured by XRR for films deposited at 300 °C were relatively stable with increasing film thickness.

The film impurities and oxide/aluminum ratio studied by TOF-ERDA in a temperature range from 110 to 300 °C for 300 nm $Al_2O_3$ are presented in Figure 2. The amount of hydrogen and carbon decreased with increasing growth temperature. The $Al_2O_3$ grown at 110 °C contained 11.3 at. % of residual hydrogen, and for film grown at 300 °C it decreased to 1 at. %. With increasing ALD temperature carbon content decreased from 0.94 to 0.18 at. %. The O/Al-ratio remained stoichiometric $Al_2O_3$ regardless of growth temperature. There was strong negative correlation between the density/refractive index of ALD $Al_2O_3$ and hydrogen and carbon content as the density/refractive index increased with decreasing impurity content; this accords with literature data [56].

## *B. Residual stress*

Residual stress of ALD $Al_2O_3$ was measured as a function of film thickness and growth temperature. The films were measured to be under tensile stress and there was no directionality detected parallel and perpendicular to the wafer flat.

The residual stress of ALD $Al_2O_3$ grown at 300 °C as a function of film thickness is presented in Figure 3a. Films were grown using (0.1-1.0-0.1-1.0) s pulse sequence. For films thicker than 100 nm, the residual stress was constant at about 230 MPa irrespective of the film thickness. For thinner films, the measurement error increased strongly, making it impossible to determine whether the residual stress depends on the film thickness.

Figure 3b presents the residual stress of 100 nm thick $Al_2O_3$ as a function of ALD temperature from 110 to 300 °C. The highest residual stress was measured on films grown at lowest temperature. Residual stress decreased from about 520 to 180 MPa with increasing temperature. The results of the two ALD reactors were alike.

To investigate the sensitivity of the residual stress of ALD $Al_2O_3$ to small changes in process conditions and post-processing steps, which might be encountered in MEMS fabrication, several parameters were varied: purge length, number of successive precursor doses, ageing time in the reactor at the growth temperature, and stability during storage in the cleanroom conditions at room temperature.

The influence of purge time was investigated on 100 nm films grown at 300 °C. By increasing the purge time from 1 to 4 s, the stress decreased from 220 to 180 MPa. This amount of stress decrease was within the typical measurement error.

The residual stress decreased with increased precursor dose, presented in Figure 4. For the film grown at 110 °C, the stress decreased from 520 to 430 MPa. Multiplication of pulses was also tested for films grown at 300 °C using two recipes with two different pulse sequences (0.1-1.0-0.1-1.0) and (0.1-4.0-0.1-4.0) s. The stress

decreased from 180 to 160 MPa with a fivefold pulsing sequence, [5x(0.1-4.0)-5x(0.1-4.0)] s. Similarly, the stress decreased from 220 to 210 MPa with a [5x(0.1-1.0)-5x(0.1-1.0)] s pulsing sequence. Although for each test series the observed decrease in residual stress was within the experimental accuracy of the measurement, the fact that a systematic decreasing trend was observed in each case, lead us to the conclusion, that the decrease in residual stress most likely had a real physical origin.

The ageing of the $Al_2O_3$ film in nitrogen was studied at the growth temperature; these were the only samples where time, at the growth temperature, after the growth was recorded. Samples grown at 300 °C in 1000 cycles (pulse sequence (0.1-1.0-0.1-1.0) s) were aged in situ by leaving them in the growth chamber after growth. Residual stress decreased from 270 to 240 MPa, when sample was aged for 18 hours at the growth temperature (reference sample was at growth temperature after processing for 20 minutes). However, this difference was within the typical measurement error.

The stability of the ALD $Al_2O_3$ during storage was studied with 100 nm thick samples grown at 110, 200 and 300 °C. Samples were stored at cleanroom conditions and the residual stress was measured as a function of storage time. Initial stress measurements were made directly after growth and repeated after 1 day, two weeks, two, three, four and six months. The residual stress for 100 nm ALD $Al_2O_3$ was stable as a function of storage time (Figure 5).

### *C. Elastic modulus and hardness*

The elastic modulus by nanoindentation was rather constant over the film thickness range from about 50 to 570 nm, presented in Table 2. The table shows also modulus value measured for the Si substrate, which was in line with literature [45].

The modulus values from nanoindentation measurement are not presented for films thinner than about 50 nm since the results carried large amount of information of the substrate at shallow indent depths. As a function of growth temperature, the modulus increased strongly for films grown at 110 to 150 °C, and saturated to around 170 GPa for films grown at higher temperatures.

The elastic modulus measured by LSAW, presented in Table 2, as a function of film thickness increased slightly over the film thickness range. Measured elastic modulus values by LSAW were in line with the nanoindentation results.

The hardness values of the film as a function of the growth temperature show a similar trend as that of the elastic modulus (Table 2). Except the one grown at 110 °C, the $Al_2O_3$ had a constant hardness value at around 10 GPa. For films thicker than 50 nm, the hardness was constant at about 10 GPa. Higher hardness values were measured for the two thinnest films. However, indentation at shallow depths can be erroneous due to tip rounding and high noise-to-data ratio and the high hardness recorded on the two thinnest films was likely due to measurement uncertainties. The hardness measured for the silicon substrate, about 10 GPa, is in line with the literature [57].

## *D. Adhesion*

The adhesion of the 300 nm ALD $Al_2O_3$ films grown at temperatures from 110 to 300 °C on RCA-cleaned silicon wafers was evaluated by scratch adhesion test. In all cases the ALD $Al_2O_3$ delamination was observed only after the cracking or breaking-up of the underlying silicon substrate, as presented in Figure 6a. The critical load for coating delamination ($L_{CALD}$) was similar for most growth temperatures, the only exception was the film grown at 150°C having slightly higher critical load. The

critical load for the Si substrate cracking, $L_{CSi}$ was lower for the uncoated reference compared to the wafers with ALD $Al_2O_3$, as presented in Figure 6b. The ALD film grown at 300 °C showed the lowest critical load value for the silicon breakage. The SEM-EDS analysis of the scratch of ALD $Al_2O_3$ grown at 300 °C (Figure 7) confirmed that $Al_2O_3$ existed on the scratch channel even after the substrate cracking took place. The SEM image also shows dark dots on $Al_2O_3$. These we suspect to originate from the blistering phenomenon also observed during annealing of ALD $Al_2O_3$ on Si [58] [59].

The SEM observation of the worn area from the scanning nanowear, on a 100 nm $Al_2O_3$ film grown at 300 °C, is presented in Figure 8. The stepwise increased set-load caused no film cracking or delamination, but increased material removal. Finally, the film was removed completely by the tip, in a single scan path with a 50 µN set-load, forming chips rather than delaminating the film. Observed chip formation indicates that the film's adhesive strength was higher than its cohesive strength. Additionally, no delamination of the film can be seen outside the scanned frames signifying excellent adhesion.

# IV. DISCUSSION

## *A. ALD growth*

The growth of $Al_2O_3$ is based on the following net reaction: 2 $Me_3Al$ (g) + 3 $H_2O$ (g) $\rightarrow$ $Al_2O_3$ (s) + 6 $CH_4$ (g). This process is one of the most studied ALD processes [1][3][8] and many of the mechanistic details have been sorted out [60][61][62][63][51]. In the next two sections, the various aspects of the process are described in a qualitative way, and when different views are present in the literature,

these are pointed out. After that, our results are interpreted in terms of the basic mechanisms.

In ALD, the net reaction is separated into two separate half-reactions. The first half-reaction is the reaction of gaseous $Me_3Al$ with an oxide surface, containing hydroxyl groups (–OH) and oxygen bridges (–O–). With –OH groups, $Me_3Al$ reacts through the ligand exchange reactions, where $CH_4$ is released and a surface-bonded –$AlMe_2$ surface species is left behind [51][60][61][62][63]. On surfaces short on OH groups, $Me_3Al$ can also react dissociatively with oxygen bridges, giving adsorbed –$AlMe_2$ and Me bonded to surface Al (Al–Me), as shown experimentally [61] and through calculations [62]; –OH groups are not necessarily needed for the reaction to occur. The –$AlMe_2$ can react further with either –OH groups or oxygen bridges, losing more methyl groups as methane or surface Al–Me [51][60][61][62][63]. As a result, the surface may contain –$AlMe_x$, with $x = 0, 1, 2$. The $Me_3Al$ reaction continues until practically all OH groups have been consumed (at low temperatures, not all OH may be able to react); the amount of Al bonded and thus the growth per cycle, GPC depends on the OH group concentration [63] [62] [64].

Different views can be found in the literature on the role of the methyl groups in the $Me_3Al$ reaction on $Al_2O_3$. According to one view [61] [65] [63] [62] [66], the reaction stops when a dense methyl group shroud is formed, where steric repulsion between neighbouring Me groups blocks further $Me_3Al$ molecules from reacting. Experiments show that the amount of methyl groups after the $Me_3Al$ reaction is about 5–6 $nm^{-2}$ on alumina, independent of ALD temperature (within 80 to 300 °C) or the alumina substrate pre-treatment temperature (200 to 800 °C) [61][63][65]. According to another view [3], also the resulting methyl group coverage decreases strongly with

temperature, and this has also a decreasing effect on the GPC. This conclusion originates from a study where $Me_3Al$ was reacted with porous alumina at 27 °C and thereafter annealed up to about 550 °C, and linear decrease of the methyl group concentration with increasing annealing temperature was seen [60]. According to the first view [61][62][63][65][66], the release of –Me as methane during annealing would free space on the surface, and $Me_3Al$ adsorption would take place again, until the methyl group shroud covers the surface. With the exception of this detail, different sources in general agree on the reactions occur during the $Me_3Al$ reaction.

The second half-reaction is the reaction of gaseous $H_2O$ reaction with the $Al_2O_3$ surface terminated with the $–AlMe_x$ surface species. With –Al–Me groups, $H_2O$ reacts through the ligand exchange reactions, where $CH_4$ is released and a surface-bonded –Al–OH groups left behind. This reaction pathway obviously saturates when the –Al–Me groups have been consumed. The $H_2O$ reaction can continue thereafter in several ways: $H_2O$ can dissociate on oxygen bridges, to form two –OH groups; neighbouring –OH groups can condense to release $H_2O$ and leave behind an oxygen bridge; and $H_2O$ can adsorb associatively through a coordination bond to metals (–Al:$OH_2$). At a certain temperature, there is limit to how dense a packing of –OH groups is stable on the surface, and this –OH group density should be the maximum obtainable also in ALD processes. It is not self-evident, however, that this maximum obtainable –OH group density would always be obtained in the ALD process. Indeed, there is evidence that at least in some studies, the $H_2O$ reactions has remained partly unsaturated. Matero et al. [50] showed for this $Al_2O_3$ process—and several other metal oxide processes—that it is possible to achieve several apparent saturated GPC levels (“growth rates”) for the same process at the same temperature by using different doses of $H_2O$. Wind and George [64] made a low-temperature study

(125 °C) for the $Me_3Al/H_2O$ process and concluded that both the $Me_3Al$ and the $H_2O$ reaction are difficult to completely saturate because of slow surface processes.

In this work, it was noticed that the GPC of the $Me_3Al/H_2O$ process increased when the purge time was shortened (4 to 1 s) at 300 °C. Too short purge times would lead to continuous CVD and decrease the layer uniformity, but that was not the case here, as the standard deviation of film thickness remained the same (1% for 100 nm films). Considering the possible reversibility of the $H_2O$ reaction, it is evident that a shorter purge time might increase the results amount of material deposited, if desorption of reversibly chemisorbed $H_2O$ occurs during purging. Such trend of increasing GPC with shorter cycle time was indeed observed in this work. On the basis of the stress measurements, the layer properties remained the same, despite the change in GPC.

In this work, it was also noticed that GPC increased especially at low temperatures when the $Me_3Al$ and $H_2O$ doses were increased (made about fivefold by repeated pulsing). The increase in GPC was significant for growth at 110 °C (~60%) and less significant but still notable at 300 °C (~10%, for both the standard recipe and the fast recipe). At the same time, the film uniformity improved, especially at low temperatures: for growth at 110 °C, the non-uniformity decreased from about 3% to 2%. Both the increasing GPC as well as the improved film uniformity indicate that the reactions had not in practice completely saturated with the basic set of dosing, especially at the lower temperature. We note that our current results do not reveal, which one of the reactions ($Me_3Al$ or $H_2O$) was partly unsaturated, or were they perhaps both unsaturated.

The fact that partly unsaturated growth was concluded to have occurred in this work especially at low temperatures (110 °C) may lead one to more general

conclusions. In this work, the GPC-vs-temperature curve for the $Me_3Al/H_2O$ process was similar as observed in many other studies (GPC increases with temperature, goes through a maximum, and decreases again) [49][50][51][52].Also the absolute values were similar, around 0.1 nm and below. It is likely that in other works also, where a similar trend is seen in the GPC-vs-temperature as in this work, the points at least on the rising part of the GPC-vs-temperature curve correspond to partly unsaturated growth. Such a trend is easily obtained when a constant pulsing scheme is used for the entire ALD temperature range, as often used in ALD studies and also in this work.

## *B. Stress*

The $Al_2O_3$ films were measured to be under tensile stress, in agreement with earlier results [14][21][22] [23][24]. Comparison of published $Al_2O_3$ stress results as a function of ALD temperature is presented in Figure 9. Stress behavior was alike; in all cases tensile residual stress of ALD $Al_2O_3$ decreased with increasing temperature. Krautheim et al. [21] has even reached a near zero residual stress value for a ALD $Al_2O_3$ grown at 500 °C. For $Me_3Al$ this temperature is problematic as it already decomposes at 330 °C [61].

The influence of thermal stress was estimated, to figure out how much of the stress was of thermal origin, using earlier published values [24] for Poisson's ratio $\upsilon_f$ and thermal expansion coefficients $\alpha_f$ and $\alpha_s$ for the ALD $Al_2O_3$ and silicon, respectively ($\upsilon_f = 0.24$, $\alpha_f = 4.2$ ppm/°C and $\alpha_s = 3.0$ ppm/°C). For elastic modulus, $E_f$ value of 171 GPa was used for films grown at 150 – 300 °C and 139 GPa for film grown at 110 °C. The wafer curvature is dependent on thermal expansion coefficients of the substrate and the film and the temperature difference between the ambient and growth temperature as follows [24]

$$\left(\frac{1}{R_1}-\frac{1}{R_0}\right)=\frac{6(1-\upsilon_s)}{E_s}\frac{t_f}{t_s^2}\frac{E_f}{(1-\upsilon_f)}(\alpha_s-\alpha_f)\Delta T\ . \tag{6}$$

The influence of the thermal stress was calculated by applying Equation 6 to Equation 1.

$$\sigma_T=\frac{E_f}{(1-\upsilon_f)}(\alpha_s-\alpha_f)\Delta T\ . \tag{7}$$

The influence of thermal stress was estimated larger for films grown at higher temperatures, outlined in Figure 9. At a growth temperature of 300 °C, about half of the total stress was from thermal origin, as for films grown at 110 °C thermal stress explains only one tenth of the total stress.

The stress of $Al_2O_3$ films remained stable during air exposure for several months, which is beneficial for MEMS processing as the film properties are (in this respect) insensitive to the time between the process steps.

## C. Elastic modulus and hardness

The elastic modulus by nanoindentation was almost constant for films grown at temperatures from 150 to 300°C; growth at 110°C gave lower values. Comparison to the film density measured by XRR is shown in Figure 10a. Elastic modulus increased with increasing density. Elastic modulus increased also with decreasing hydrogen impurity content (see Tables 1 and 2). The results are consistent with the principle that elastic modulus of a material is depending on density of atomic bonds [67]. A comparison of our results to the published elastic modulus values, presented in Figure 11 shows in general good agreement (considering the measurement uncertainty). Unlike earlier publications, in which the modulus of the film was concluded to increase with increasing growth temperature [10][29], our results do not

show a continuously increasing elastic modulus but one that saturated to a certain level. The main reason for the different conclusion for the temperature dependency is most likely that our experiments covered a wider temperature range with more samples than in earlier studies, allowing more subtle changes to be observed.

LSAW gave similar elastic modulus values as nanoindentation. Interestingly, elastic modulus measured by LSAW increased slightly with increasing film thickness, indicating that small changes in film properties occurred.

Similarly as the elastic modulus, hardness was also nearly constant as a function of film thickness, increasing with increasing film density (Figure 10b) and decreasing with increasing hydrogen content (see Tables 1 and 2). There are more discrepancies of the film hardness between the results of this study and those from the literature (Figure 12). For films grown at temperatures from 150 to 300 °C we obtained hardness values about constant at 10 GPa, while literature shows values from 6 to 12 GPa. Growth at 110 °C gave lower value of about 8 GPa. The possible reasons for the differences range from the differences in measurement setup to differences in ALD growth.

## *D. Adhesion*

The results from both the scratch adhesion test and scanning nanowear suggest strong adhesion of the $Al_2O_3$ films to the RCA-cleaned silicon. In the scratch adhesion test, the coating delamination was observed only after the cracking and breaking-up of the silicon substrate (Figure 6a). Even after silicon cracking the coating was mostly detached onto the substrate even in the scratch channel. Since the observed delamination was related to silicon cracking, it was not clear to what extent the adhesion failure between the film and substrate was influenced by the silicon

breakage. On the other hand, the ALD films clearly increased the critical load for the silicon breakage and, therefore, enhanced the load carrying capacity of the silicon substrate system (Figure 6a and 6b).

The influence of the ALD temperature to the substrate breakage and film delamination was inconsistent. The critical loads of the silicon breakage and film delamination for the films grown at 110, 200 and 250 °C were rather similar (Fig. 6A and B). However, the $L_{CSi}$ was slightly higher for the film grown at 150 °C and clearly lower for the one at 300 °C (Fig. 6A and B). The reason of this inconsistence is unclear at this stage and repeated tests are needed to ensure the phenomena and improve the statistics of the experiment data.

The chip formation and no observable delamination of the film in the nanowear test indicated excellent film adhesion to the substrate. Peeling off in chips instead of spalling off by delamination suggests that the film adhesion to the substrate was higher than its cohesion. The origin of the strong adhesion of $Al_2O_3$ on thermally-grown $SiO_2$ or thin $SiO_x$ on Si has been observed and attributed to the formation of silicate-type bonding, Si–O–Al [36][38]. The growth of $Al_2O_3$ from $AlMe_3$ and $H_2O$ has been widely studied and the reaction mechanism has been widely reviewed [1]. Most typically, Si–O–Al bonds form when $AlMe_3$ reacts with Si–OH groups (one or several), to give Si–O–$AlMe_x$ surface species ($x = 0, 1, 2$) and release one or several methane molecules [68][69]. In an alternative reaction path which should be active at least when Si–OH groups are less abundant (e.g. on thermally-grown $SiO_2$), reaction occurs also with surface Si–O–Si bridges, also generating Si–O–$AlMe_x$ surface species, but instead of releasing a gaseous reaction product, leaving behind surface Si–$Me_y$ species (y = 1, 2, 3) [68][69]. Evidently, the Si–O–Al bonds account for the

strong adhesion observed also in this work and the type of bonding seems independent of the growth temperature.

# V. CONCLUSIONS

In this work, the stress, elastic modulus, hardness and adhesion of the ALD $Al_2O_3$ thin films made from $Me_3Al$ and $H_2O$ on RCA-cleaned Si were characterized as a function of growth temperature (110 to 300 °C) and film thickness (10 to 600 nm). Supporting physicochemical characterization was made to assist the interpretations. The ALD $Al_2O_3$ films were under tensile stress, in the scale of hundreds of MPa. The residual stress was alike for films grown in ALD reactors by different reactor manufacturers. The magnitude of the residual stress decreased strongly with increasing ALD temperature. At low temperatures, the residual stress was dominated by growth-related stress and this factor decreased with increasing temperature. The stress was stable during storage. Films grown at 150 to 300 °C had a fairly constant elastic modulus (ca. 170 GPa) and hardness (ca. 10 GPa). Films grown at 110 °C were softer with a lower elastic modulus. The softness at low growth temperature is at least partly explained by the higher residual hydrogen content and lower density of the films. The ALD $Al_2O_3$ films adhered strongly on the RCA-cleaned silicon.

These results provide input to MEMS design with ALD $Al_2O_3$ and will be useful to other applications of ALD $Al_2O_3$ films as well. Furthermore, as the process studied in this work is a commonly recognized model system for ALD, we hope that our results will also serve as a useful comparison point for future studies on the mechanical properties of ALD films.


# ACKNOWLEDGMENTS

OMEY thanks Leif Grönberg and Antti Tolkki for guidance given in profilometer measurements. RLP thanks Prof. Steven George for discussion on the $Al_2O_3$ ALD growth mechanism. Tatu Muukkonen is thanked for initiating the microscratch measurements. This work has been carried out within the MECHALD project funded by Tekes and is linked to the Finnish Centers of Excellence in Atomic Layer Deposition (ref. 251220) and Nuclear and Accelerator Based Physics (refs. 213503 and 251353) of the Academy of Finland. Parts of these results were presented in posters at the 12th AVS-ALD 2012 conference, June 17-20th, 2012, Dresden, Germany.

# REFERENCES


[1] R.L. Puurunen, Journal of Applied Physics 97 (2005) 121301.

[2] S.M. George, A.W. Ott, J.W. Klaus, The Journal of Physical Chemistry 100 (1996) 13121.

[3] S.M. George, Chemical Reviews 110 (2010) 111.

[4] K.-E. Elers, T. Blomberg, M. Peussa, B. Aitchison, S. Haukka, S. Marcus, Chemical Vapor Deposition 12 (2006) 13.

[5] M. Ritala, M. Leskelä, J.-P. Dekker, C. Mutsaers, P.J. Soininen, J. Skarp, Chemical Vapor Deposition 5 (1999) 7.

[6] L. Wang, J.J. Travis, A.S. Cavanagh, X. Liu, S.P. Koenig, P.Y. Huang, S.M. George, J.S. Bunch, Nano Letters 12 (2012) 3706.

[7] M. Leskelä, M. Ritala, Thin Solid Films 409 (2002) 138.

[8] V. Miikkulainen, M. Leskela□, M. Ritala, R.L. Puurunen, Journal of Applied Physics 113 (2013) 021301.

[9] R.L. Puurunen, H. Kattelus, T. Suntola, in:, V. Lindroos, M. Tilli, A. Lehto, T. Motooka (Eds.), Handbook of Silicon Based MEMS Materials and Technologies, William Andrew Publishing, Boston, 2010, pp. 433–446.

[10] C.F. Herrmann, F.W. DelRio, D.C. Miller, S.M. George, V.M. Bright, J.L. Ebel, R.E. Strawser, R. Cortez, K.D. Leedy, Sensors and Actuators A: Physical 135 (2007) 262.

[11] X.J. He, Z.Q. Lv, B. Liu, Z.H. Li, Sensors and Actuators A: Physical 188 (2012) 342.

[12] M. Blomberg, H. Kattelus, A. Miranto, Sensors and Actuators A: Physical 162 (2010) 184.

[13] A. Rissanen, U. Kantojärvi, M. Blomberg, J. Antila, S. Eränen, Sensors and Actuators A: Physical 182 (2012) 130.

[14] Y.-J. Chang, J.M. Gray, A. Imtiaz, D. Seghete, T. Mitch Wallis, S.M. George, P. Kabos, C.T. Rogers, V.M. Bright, Sensors and Actuators A: Physical 154 (2009) 229.

[15] R.L. Puurunen, T. Suni, O.M.E. Ylivaara, H. Kondo, M. Ammar, T. Ishida, H. Fujita, A. Bosseboeuf, S. Zaima, H. Kattelus, Sensors and Actuators A: Physical 188 (2012) 268.

[16] N.D. Hoivik, J.W. Elam, R.J. Linderman, V.M. Bright, S.M. George, Y.C. Lee, Sensors and Actuators A: Physical 103 (2003) 100.

[17] M.F. Doerner, W.D. Nix, CRC Critical Reviews in Solid State and Materials Sciences 14 (1988) 225.

[18] W.D. Nix, Metallurgical Transactions A 20 (1989) 2217.

[19] F. Spaepen, Acta Materialia 48 (2000) 31.

[20] S. Senturia, in:, S. Senturia (Ed.), Microsystem Design, Kluwer Academic Publishers, 2001, pp. 183–263.

[21] G. Krautheim, T. Hecht, S. Jakschik, U. Schröder, W. Zahn, Applied Surface Science 252 (2005) 200.

[22] M.K. Tripp, C. Stampfer, D.C. Miller, T. Helbling, C.F. Herrmann, C. Hierold, K. Gall, S.M. George, V.M. Bright, Sensors and Actuators A: Physical 130-131 (2006) 419.

[23] R.L. Puurunen, J. Saarilahti, H. Kattelus, ECS Transactions 11 (2007) 3.

[24] D.C. Miller, R.R. Foster, S.-H. Jen, J.A. Bertrand, S.J. Cunningham, A.S. Morris, Y.-C. Lee, S.M. George, M.L. Dunn, Sensors and Actuators A: Physical 164 (2010) 58.

[25] H.B. Profijt, M.C.M. van de Sanden, W.M.M. Kessels, Journal of Vacuum Science & Technology A: Vacuum, Surfaces, and Films 31 (2013) 01A106.

[26] V. Kaajakari, in:, Practical MEMS, 1.01 ed., Small Gear Publishing, 2009, pp. 49 – 71.

[27] M. Ohring, in:, Materials Science of Thin Films, Second edi, Academic Press, 2002, pp. 711–781.

[28] K. Tapily, J.E. Jakes, D.S. Stone, P. Shrestha, D. Gu, H. Baumgart, A.A. Elmustafa, Journal of The Electrochemical Society 155 (2008) H545.

[29] S.J. Bull, Journal of Vacuum Science & Technology A 30 (2012) 01A160.

[30] O. Hahtela, P. Sievilä, N. Chekurov, I. Tittonen, Journal of Micromechanics and Microengineering 17 (2007) 737.

[31] T.M. Mayer, J.W. Elam, S.M. George, P.G. Kotula, R.S. Goeke, Applied Physics Letters 82 (2003) 2883.

[32] K.L. Mittal, Electrocomponent Science and Technology 3 (1976) 21.

[33] S.T. Gonczy, N. Randall, International Journal of Applied Ceramic Technology 2 (2005) 422.

[34] J. Meneve, H. Ronkainen, P. Andersson, K. Verkammen, D. Camino, D.G. Teer, J. von Stabut, M.G. Gee, N.M. Jennet, J. Banks, B. Bellaton, E. Matthaei-Schultz, H. Vetters, in:, K.L. Mittal (Ed.), Adhesion Measurement of Films and Coatings, Volume 2, VSP BV, The Netherlands, 2001, pp. 79–106.

[35] J. Chen, S.J. Bull, Journal of Physics D: Applied Physics 44 (2011) 034001.

[36] J.N. Ding, X.F. Wang, N.Y. Yuan, C.L. Li, Y.Y. Zhu, B. Kan, Surface and Coatings Technology 205 (2011) 2846.

[37] T.O. Ka□a□ria□inen, P.J. Kelly, D.C. Cameron, B. Beake, H. Li, P.M. Barker, C.F. Struller, Journal of Vacuum Science & Technology A: Vacuum, Surfaces and Films 30 (2012) 01A132.

[38] J.-K. Kim, T.-H. Cheon, S.-H. Kim, Y.-B. Park, Japanese Journal of Applied Physics 51 (2012) 05EB04.

[39] K. Knapas, M. Ritala, Critical Reviews in Solid State and Materials Sciences 38 (2013) 167.

[40] M. Laitinen, T. Sajavaara, M. Rossi, J. Julin, R.L. Puurunen, T. Suni, T. Ishida, H. Fujita, K. Arstila, B. Brijs, H.J. Whitlow, Nuclear Instruments and Methods in Physics Research Section B: Beam Interactions with Materials and Atoms 269 (2011) 3021.

[41] G.G. Stoney, Proceedings of the Royal Society A: Mathematical, Physical and Engineering Sciences 82 (1909) 172.

[42] W.A. Brantley, Journal of Applied Physics 44 (1973) 534.

[43] S. Timoshenko, J. Opt. Soc. Am 11 (1925) 233.

[44] W.C. Oliver, G.M. Pharr, Journal of Materials Research 7 (1992) 1564.

[45] J.J. Worthman, R.A. Evans, Journal of Applied Physics 36 (1965) 153.

[46] A.C. Fischer-Cripps, in:, Nanoindentation, Mechanical, Springer New York, New York, NY, 2011, pp. 1–19.

[47] D. Schneider, T. Schwarz, H.-J. Scheibe, M. Panzner, Thin Solid Films 295 (1997) 107.

[48] ASTM C1624-05, (2010) 28.

[49] A.W. Ott, J.W. Klaus, J.M. Johnson, S.M. George, Thin Solid Films 292 (1997) 135.

[50] R. Matero, A. Rahtu, M. Ritala, M. Leskelä, T. Sajavaara, Thin Solid Films 368 (2000) 1.

[51] A. Rahtu, T. Alaranta, M. Ritala, Langmuir 17 (2001) 6506.

[52] M.D. Groner, F.H. Fabreguette, J.W. Elam, S.M. George, Chemistry of Materials 16 (2004) 639.

[53] J.L. van Hemmen, S.B.S. Heil, J.H. Klootwijk, F. Roozeboom, C.J. Hodson, M.C.M. van de Sanden, W.M.M. Kessels, Journal of The Electrochemical Society 154 (2007) G165.

[54] J.M. Rafí, M. Zabala, O. Beldarrain, F. Campabadal, Journal of The Electrochemical Society 158 (2011) G108.

[55] G. Dingemans, M.C.M. van de Sanden, W.M.M. Kessels, Electrochemical and Solid-State Letters 13 (2010) H76.

[56] R. Matero, Atomic Layer Deposition of Oxide Films - Growth, Characterisation and Reaction Mechanism Studies, University of Helsinki, 2004.

[57] N. Panich, KMITL Sci. J. 5 (2005) 483.

[58] R.L. Puurunen, J. Kiihamäki, H. Kattelus, in:, AVS Topical Conference on Atomic Layer Deposition, San Jose, California 8-10 August, American Vacuum Society, San Jose, 2005.

[59] O. Beldarrain, M. Duch, M. Zabala, J.M. Rafí, M.B. González, F. Campabadal, Journal of Vacuum Science & Technology A: Vacuum, Surfaces, and Films 31 (2013) 01A128.

[60] A.C. Dillon, A.W. Ott, J.D. Way, S.M. George, Surface Science 322 (1995) 230.

[61] R.L. Puurunen, M. Lindblad, A. Root, A.O.I. Krause, Physical Chemistry Chemical Physics 3 (2001) 1093.

[62] S.D. Elliot, J.C. Greer, Journal of Materials Chemistry 14 (2004) 3246.

[63] R.L. Puurunen, Applied Surface Science 245 (2005) 6.

[64] R.A. Wind, S.M. George, The Journal of Physical Chemistry A 114 (2010) 1281.

[65] R.L. Puurunen, Preparation by Atomic Layer Deposition and Characterisation of Catalyst Supports Surfaced with Aluminium Nitride, Helsinki University of Technology, 2002.

[66] S.D. Elliott, H.P. Pinto, Journal of Electroceramics 13 (2004) 117.

[67] M.F. Ashby, Acta Metallurgica 37 (1989) 1273.

[68] E.-L. Lakomaa, A. Root, T. Suntola, Applied Surface Science 107 (1996) 107.

[69] R.L. Puurunen, A. Root, S. Haukka, E.I. Iiskola, M. Lindblad, A.O.I. Krause, The Journal of Physical Chemistry B 104 (2000) 6599.

# LIST OF TABLE CAPTIONS

Table 1. Reflectometer, ellipsometer and XRR results presented for $Al_2O_3$ grown in Picosun[TM] R-150 ALD reactor.

Table 2. Elastic modulus and hardness of the ALD $Al_2O_3$ films. The error limits represent one standard deviation.

# LIST OF FIGURE CAPTIONS

Figure 1 (a) The average thickness of 49 points reflectometer measurement as a function of ALD cycles for ALD $Al_2O_3$ grown at 300 °C on $SiO_x$ terminated silicon. The pulse sequence for $Al_2O_3$ growth was 0.1 s for reactions and 1.0 s for purges. (b) The average thickness per cycles presented as a function of growth temperature for films grown in the Picosun$^{TM}$ R-150 reactor. Pulse sequences were 0.1-4.0-0.1-4.0 s and 0.1-1.0-0.1-1.0 s.

Figure 2. Impurity (hydrogen and carbon) concentrations and O/Al ratio of ALD $Al_2O_3$ as a function of ALD temperature analyzed with TOF-ERDA. Targeted film thickness was 300 nm.

Figure 3. The residual stress of the ALD $Al_2O_3$ as a function of (a) film thickness and (b) growth temperature. In (a) films were deposited at 300 °C, using TMA-purge-$H_2O$-purge sequence of (0.1-1.0-0.1-1.0) s. The symbols present median stress values and bars present calculated maximum error values. In (b) the film thickness was kept constant at 100 nm and the TMA-purge-$H_2O$-purge sequence for films grown at Reactor A (Picosun$^{TM}$ R-150) was (0.1-4.0-0.1-4.0) s and at Reactor B: (BENEQ TFS-500) (0.25-0.75-0.2-0.75) s. The symbols present median stress values and bars present calculated maximum error values.

Figure 4. The residual stress of the 100 nm ALD $Al_2O_3$ as a function of repeated precursor pulses in the Picosun$^{TM}$ R-150 reactor. The number of the sequential pulses was increased by 5 and growths were done at 110 and 300 °C. The symbols present median stress values and bars present calculated maximum error values.

Figure 5. Residual stress as a function of storage time for 100 nm ALD $Al_2O_3$ deposited at 110, 200 and 300 °C in the Picosun$^{TM}$ R-150 reactor. The pulsing sequence was (0.1-4.0-0.1-4.0) s. The symbols present median stress values.

Figure 6 (a) Comparison of the optical panorama images from the scratches on reference silicon and on the samples with ALD $Al_2O_3$ grown at 110 – 300 °C. The vertical black lines indicate the breakage point of the Si substrate ($L_{CSi}$) and the short lines indicate the first visible film delamination ($L_{CALD}$). In (b) the critical loads for the Si breakage, $L_{CSi}$,

and for the ALD $Al_2O_3$ delamination, $L_{CALD}$, as an average value of three measurements. The error bars indicate the smallest and highest values of the measurements.

Figure 7. SEM image and EDS analysis of the scratch channel of about 300 nm $Al_2O_3$ grown at 300 °C on silicon showing the breakage point of Si substrate. EDS signals from the scratch channel before (1) and after (2) the breakage show the existence of $Al_2O_3$ film on the scratch channel after the breakage point. Signal no. 3 represents a reference analysis of the coated surface.

Figure 8. SEM image of scanning nanowear testing of about 100 nm ALD $Al_2O_3$ on silicon. Right: Increased scanning load of 10, 20, 30 and 40 µN in a single frame of 3x3 µm. Left: 50 µN scanning load used in a single frame of 3x3 µm. Around tested area chips cut from the coating can be seen. The coating was removed completely with the scanning load of 50 µN. No delamination of the coating can be seen outside the scanned frames signifying excellent adhesion.

Figure 9. Comparison of our results to published data for the residual stress of ALD $Al_2O_3$ as function of ALD temperature. Symbols (■) and (●) refer to results presented in this work and are median stress values, bars present calculated maximum error values. The dashed line presents estimation of thermal stress component. References for earlier published data are for Krautheim et al. [21], Tripp et al.[22], Puurunen et al. [23], Chang et al. [14] and Miller et al. [24].

Figure 10 (a). Elastic modulus as a function of ALD $Al_2O_3$ density. (b) Hardness measured by nanoindentation as a function of the film density. Growth temperatures are recorded in graph.

Figure 11. Comparison of our results of elastic modulus values for ALD $Al_2O_3$ with published values. References for earlier published data are for Tripp et al. [22], Hermann et al. [10], Hahtela et al. [30], Tapily et al. [28], Miller et al. [24], Ding et al. [36] and Bull [29]. Our data presents error limits that are standard deviation values.

Figure 12. Comparison of our hardness values measured by nanoindentation for ALD $Al_2O_3$ with published hardness values. References for earlier published data are for Tripp

et al. [22], Hermann et al. [10], Tapily et al. [28], Miller et al. [24], Ding et al. [36] and Bull [29].

**Table 1**

Table 1. Reflectometer, ellipsometer and XRR results presented for $Al_2O_3$ grown in Picosun$^{TM}$ R-150 ALD reactor.

| Growth temperature [°C ] | Pulse sequence [s] | Growth cycles | Reflectometer thickness (49 pts) [nm] | Thickness/ cycles [nm] | St.dev. (49 pts) [nm] | St. dev. (49 pts) [%] | Ellipsometer thickness (5pts) [nm] | Refractive index (5 pts) | XRR thickness [nm] | XRR density [g/cm3] | XRR roughness [nm] |
|---|---|---|---|---|---|---|---|---|---|---|---|
| 110 | 0.1-4.0-0.1-4.0 | 1283 | 93.9 | 0.073 | 2.6 | 2.8 | 95.4 | 1.615 | - | - | - |
| 110 | 5(0.1-4.0)-5(0.1-4.0) | 1283 | 152.4 | 0.119 | 2.9 | 1.9 | | | | | |
| 110 | 0.1-4.0-0.1-4.0 | 3933 | 288.3 | 0.073 | 7.7 | 2.7 | - | - | - | 2.85 | - |
| 150 | 0.1-4.0-0.1-4.0 | 1137 | 95.6 | 0.084 | 2.3 | 2.4 | 96.1 | 1.638 | - | - | - |
| 150 | 0.1-4.0-0.1-4.0 | 3411 | 285.4 | 0.084 | 6.2 | 2.2 | - | - | - | 2.95 | - |
| 200 | 0.1-4.0-0.1-4.0 | 1037 | 96.2 | 0.093 | 1.7 | 1.8 | 96.0 | 1.649 | - | - | - |
| 200 | 0.1-4.0-0.1-4.0 | 3120 | 286.7 | 0.092 | 4.9 | 1.7 | - | - | - | 3.05 | - |
| 250 | 0.1-4.0-0.1-4.0 | 1037 | 97.1 | 0.094 | 1.5 | 1.5 | 96.4 | 1.655 | - | - | - |
| 250 | 0.1-4.0-0.1-4.0 | 3115 | 291.9 | 0.094 | 3.9 | 1.3 | - | - | - | 3.10 | - |
| 300 | 0.1-1.0-0.1-1.0 | 100 | 9.9 | 0.099 | 0.2 | 2.0 | - | - | 9.8 | 3.10 | 0.6 |
| 300 | 0.1-1.0-0.1-1.0 | 200 | 19.8 | 0.099 | 0.3 | 1.5 | - | - | 19.5 | 3.15 | 0.6 |
| 300 | 0.1-1.0-0.1-1.0 | 500 | 48.5 | 0.097 | 0.6 | 1.2 | - | - | 48.5 | 3.10 | 0.5 |
| 300 | 0.1-1.0-0.1-1.0 | 1000 | 96.1 | 0.096 | 1.0 | 1.0 | - | - | 96.1 | 3.10 | 0.5 |
| 300 | 5(0.1-1.0)-5(0.1-1.0) | 1009 | 107.9 | 0.107 | 1.0 | 0.9 | | | | | |
| 300 | 0.1-4.0-0.1-4.0 | 1109 | 99.5 | 0.090 | 1.0 | 1.0 | 99.2 | 1.657 | - | - | - |
| 300 | 5(0.1-4.0)-5(0.1-4.0) | 1109 | 111.2 | 0.100 | 1.0 | 0.9 | | | | | |
| 300 | 0.1-1.0-0.1-1.0 | 3000 | 283.7 | 0.095 | 3.3 | 1.2 | - | - | 295 | 3.10 | 0.8 |
| 300 | 0.1-1.0-0.1-1.0 | 6000 | 566.9 | 0.094 | 6.5 | 1.1 | - | - | - | 3.10 | - |

**Table 2**

Table 2. Elastic modulus and hardness results presented for $Al_2O_3$ grown in Picosun$^{TM}$ R-150 ALD reactor. The error limits represent one standard deviation.

| Growth temperature [°C] | Pulse sequence [s] | Growth cycles | Thickness [nm] | Elastic modulus by nanoindentation [GPa] | Elastic modulus by LSAW [GPa] | Hardness [GPa] |
|---|---|---|---|---|---|---|
| (Si ref) | – | – | – | 153.7±6.4 | – | 10.2±0.4 |
| 110 | 0.1-4-0.1-4 | 3933 | 288.3 | 138.5±8.4 | – | 7.9±0.2 |
| 150 | 0.1-4-0.1-4 | 3411 | 285.4 | 171.2±11.6 | – | 10.0±0.2 |
| 200 | 0.1-4-0.1-4 | 3120 | 286.7 | 166.6±10.7 | – | 9.8±0.3 |
| 250 | 0.1-4-0.1-4 | 3115 | 291.9 | 178.0±14.4 | – | 11.1±0.7 |
| 300 | 0.1-1-0.1-1 | 100 | 9.9 | – | 170.2±2.8 | 13.8±0.9 |
| 300 | 0.1-1-0.1-1 | 200 | 19.8 | – | 169.4±1.6 | 13.3±0.4 |
| 300 | 0.1-1-0.1-1 | 500 | 48.5 | 166.2±10.3 | 173.1±0.6 | 10.1±0.3 |
| 300 | 0.1-1-0.1-1 | 1000 | 96.1 | 172.9±9.4 | 174.7±0.2 | 10.4±0.4 |
| 300 | 0.1-1-0.1-1 | 3000 | 283.7 | 169.8±9.8 | 175.0±0.8 | 10.5±0.5 |
| 300 | 0.1-1-0.1-1 | 6000 | 566.9 | 172.8±10.8 | 176.0±1.0 | 10.3±0.6 |

Figure 1A

Click here to download Figures (if any): Figure 1A.eps

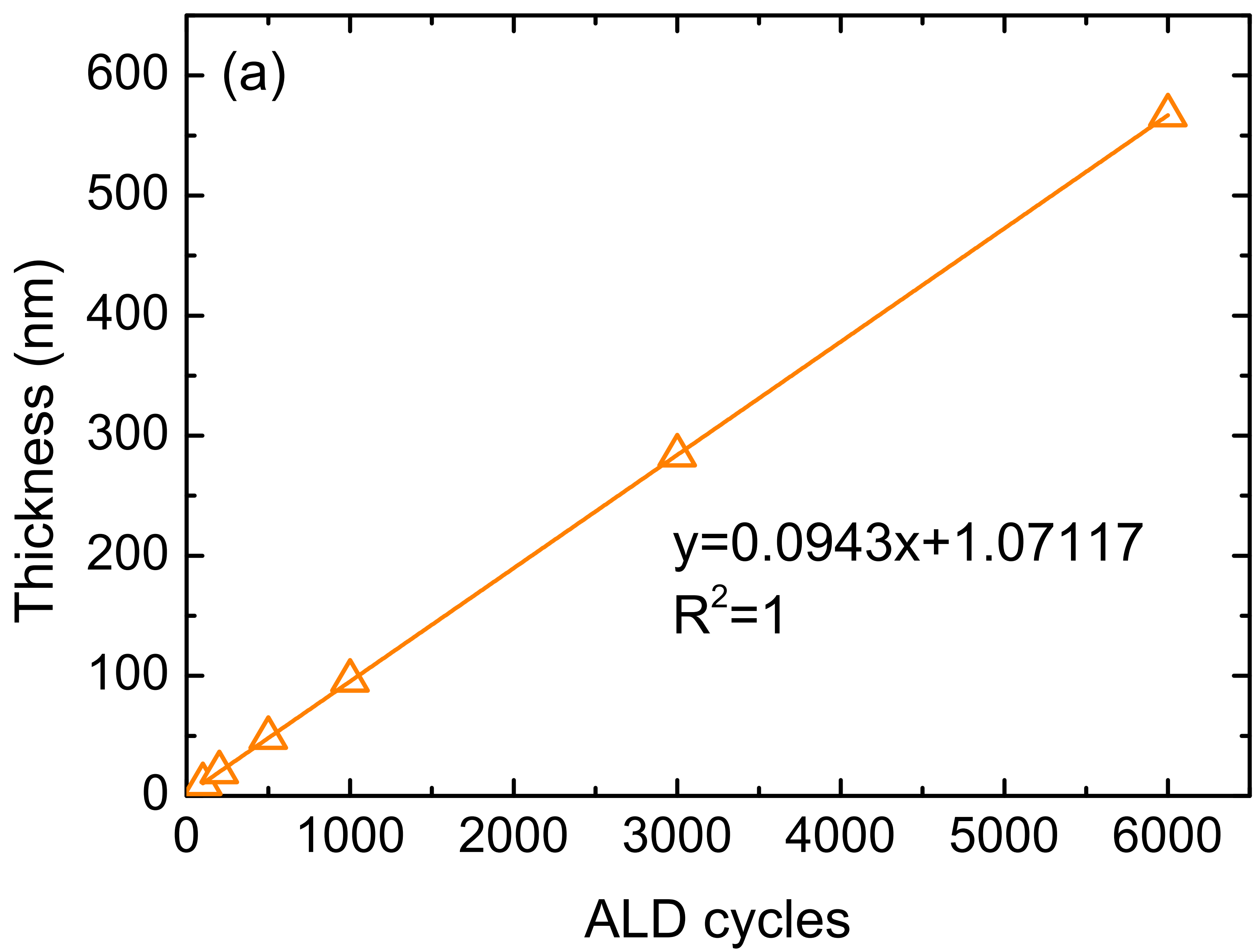

Figure 1B

Click here to download Figures (if any): Figure 1B.eps

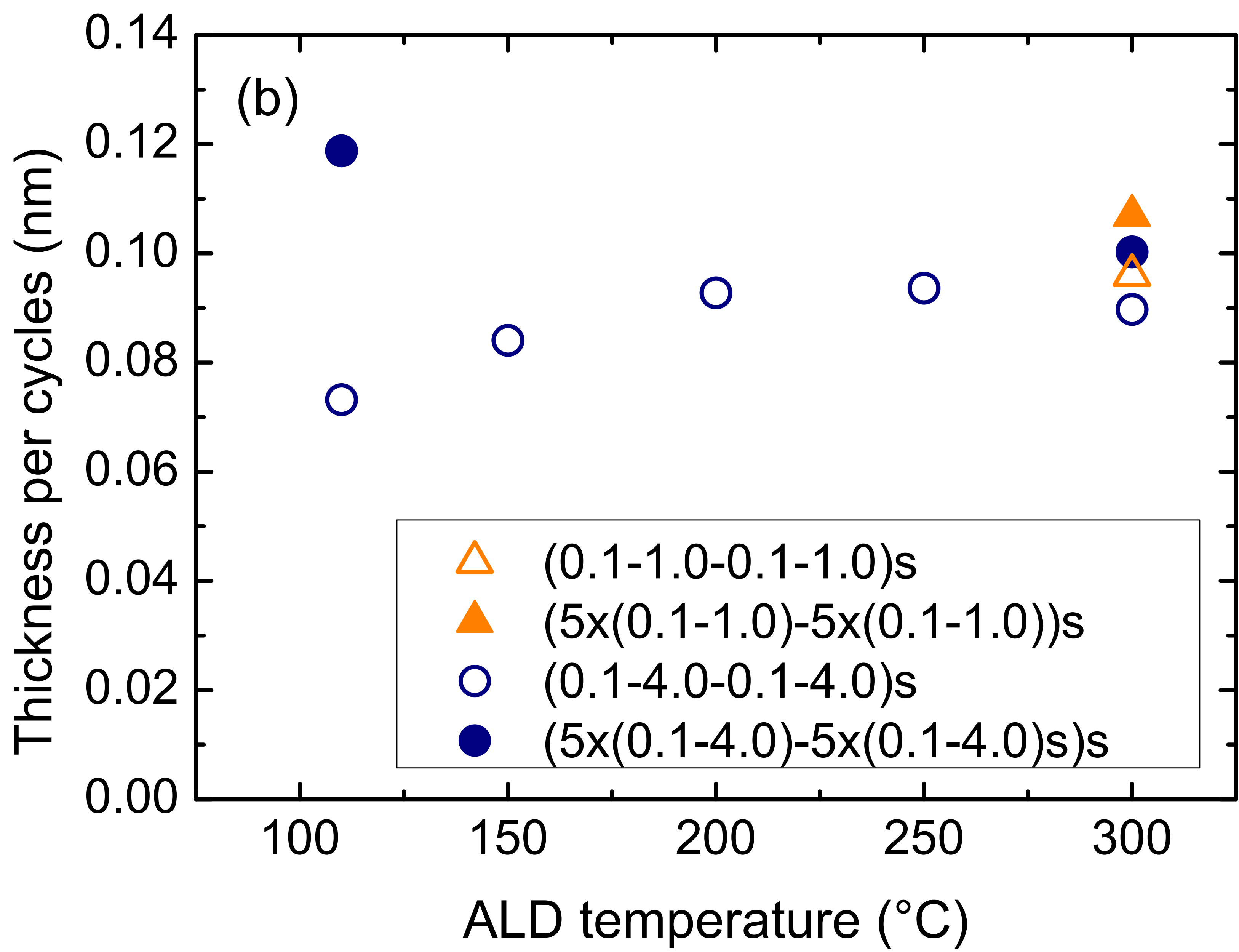

Figure 2
Click here to download Figures (if any): Figure 2.eps

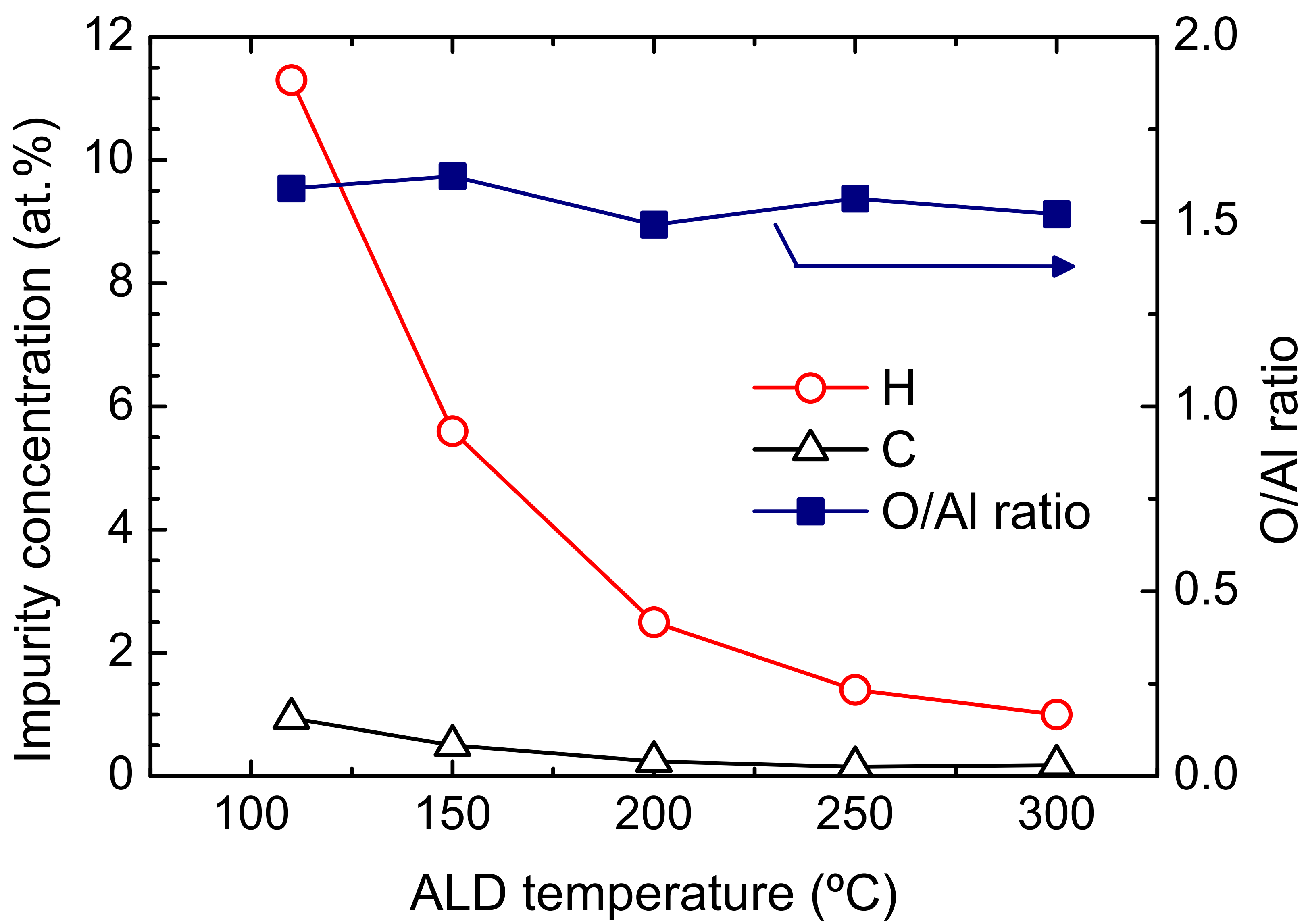

Figure 3A

Click here to download Figures (if any): Figure 3A.eps

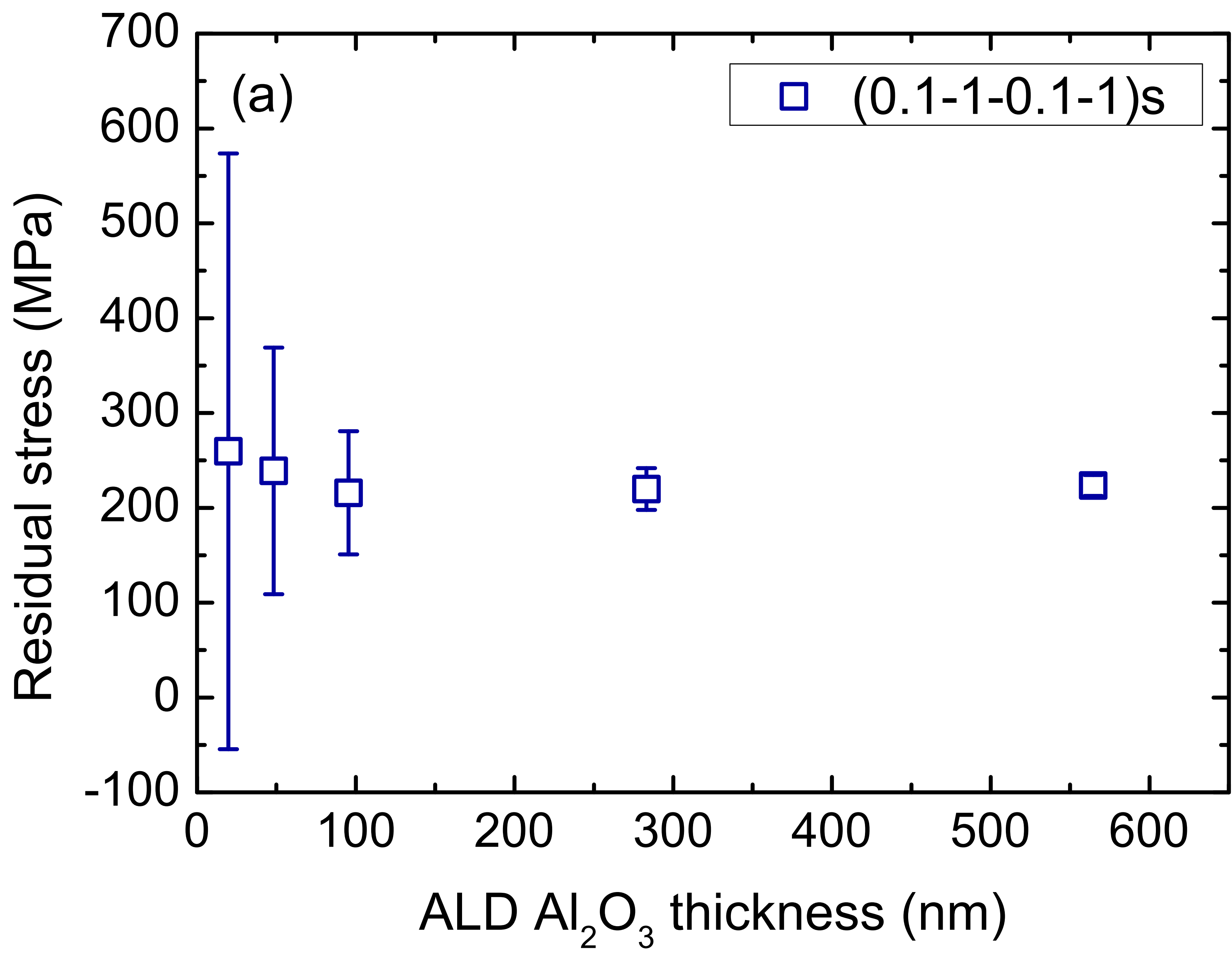

Figure 3B

Click here to download Figures (if any): Figure 3B.eps

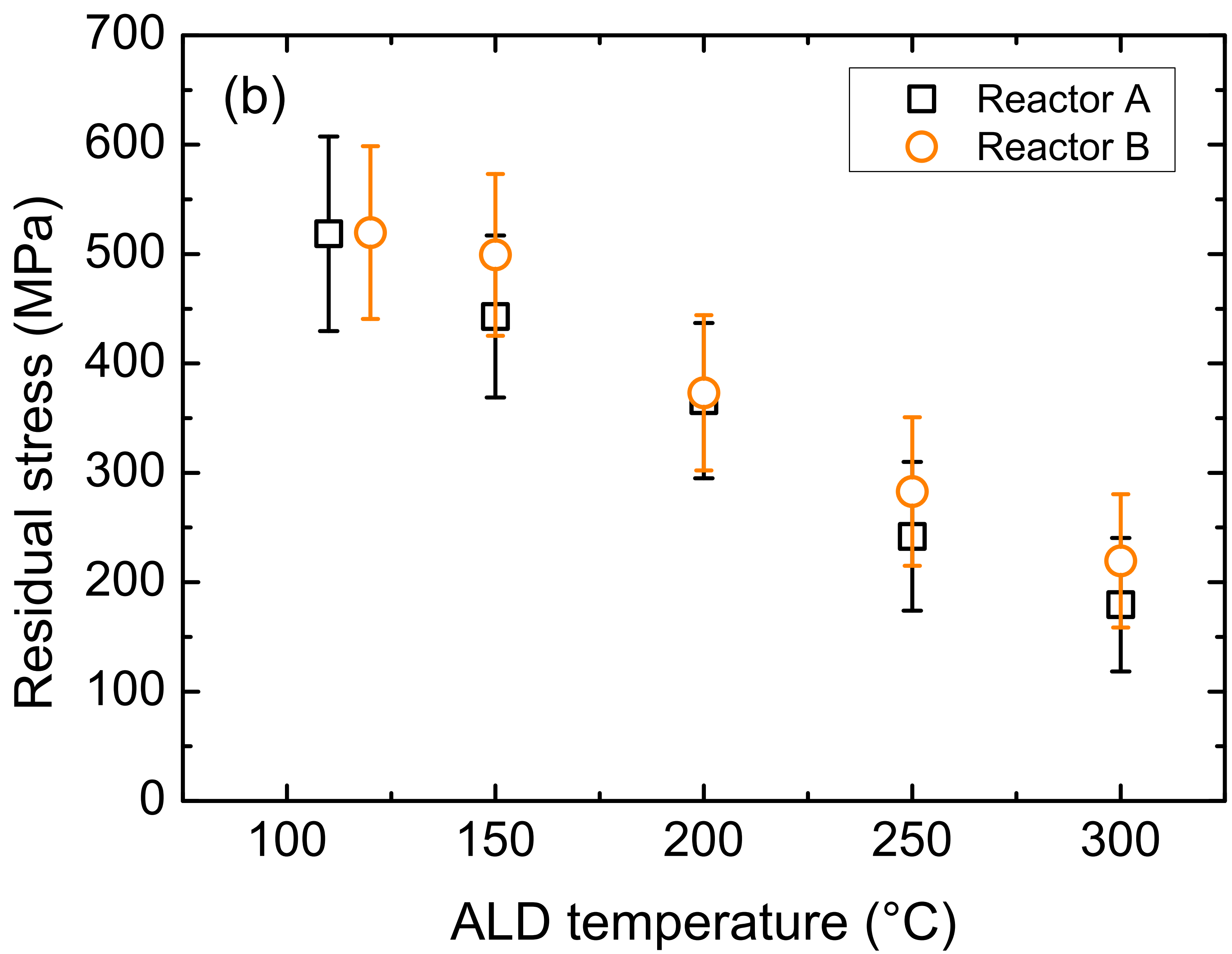

Figure 4
Click here to download Figures (if any): Figure 4.eps

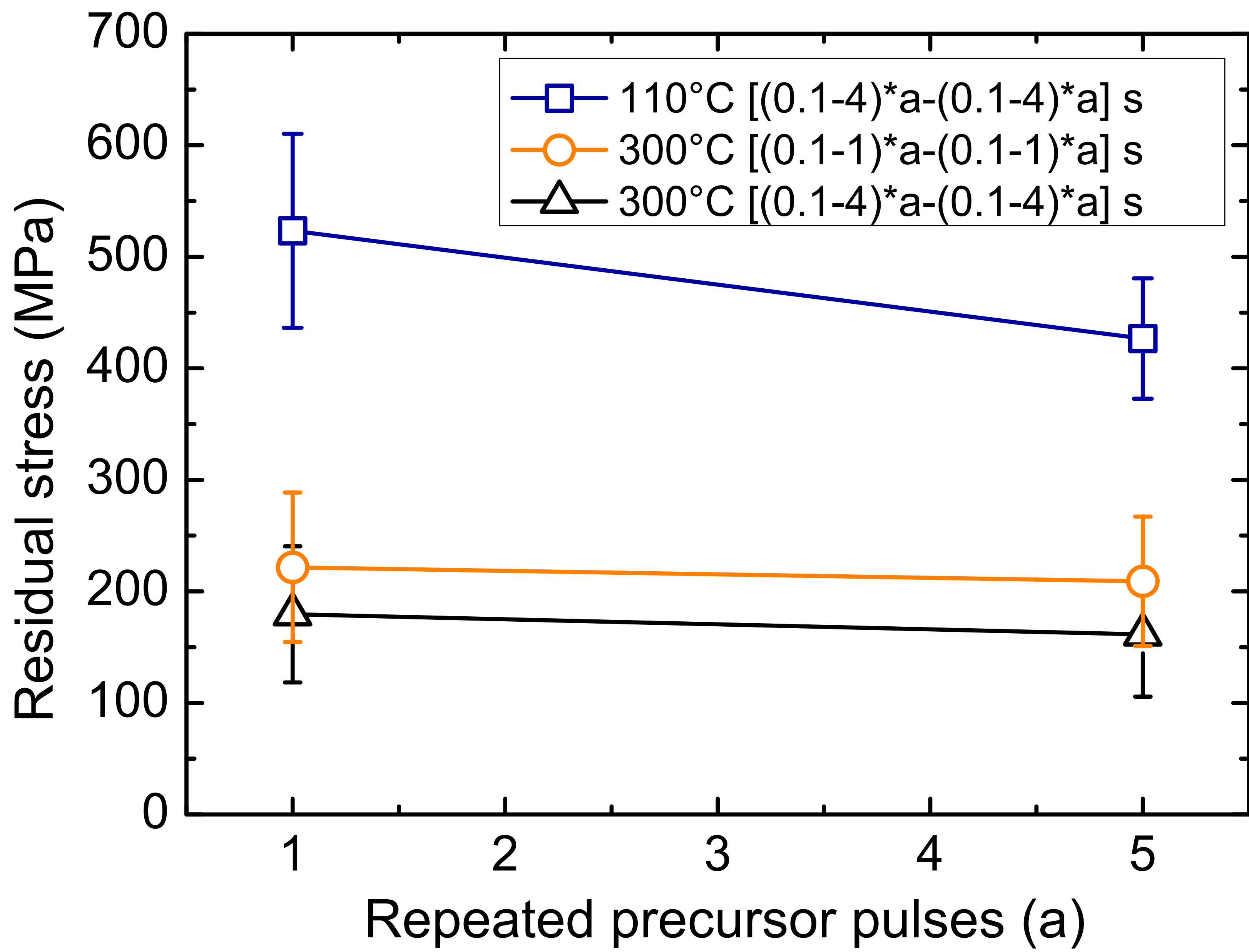

Figure 5

Click here to download Figures (if any): Figure 5.eps

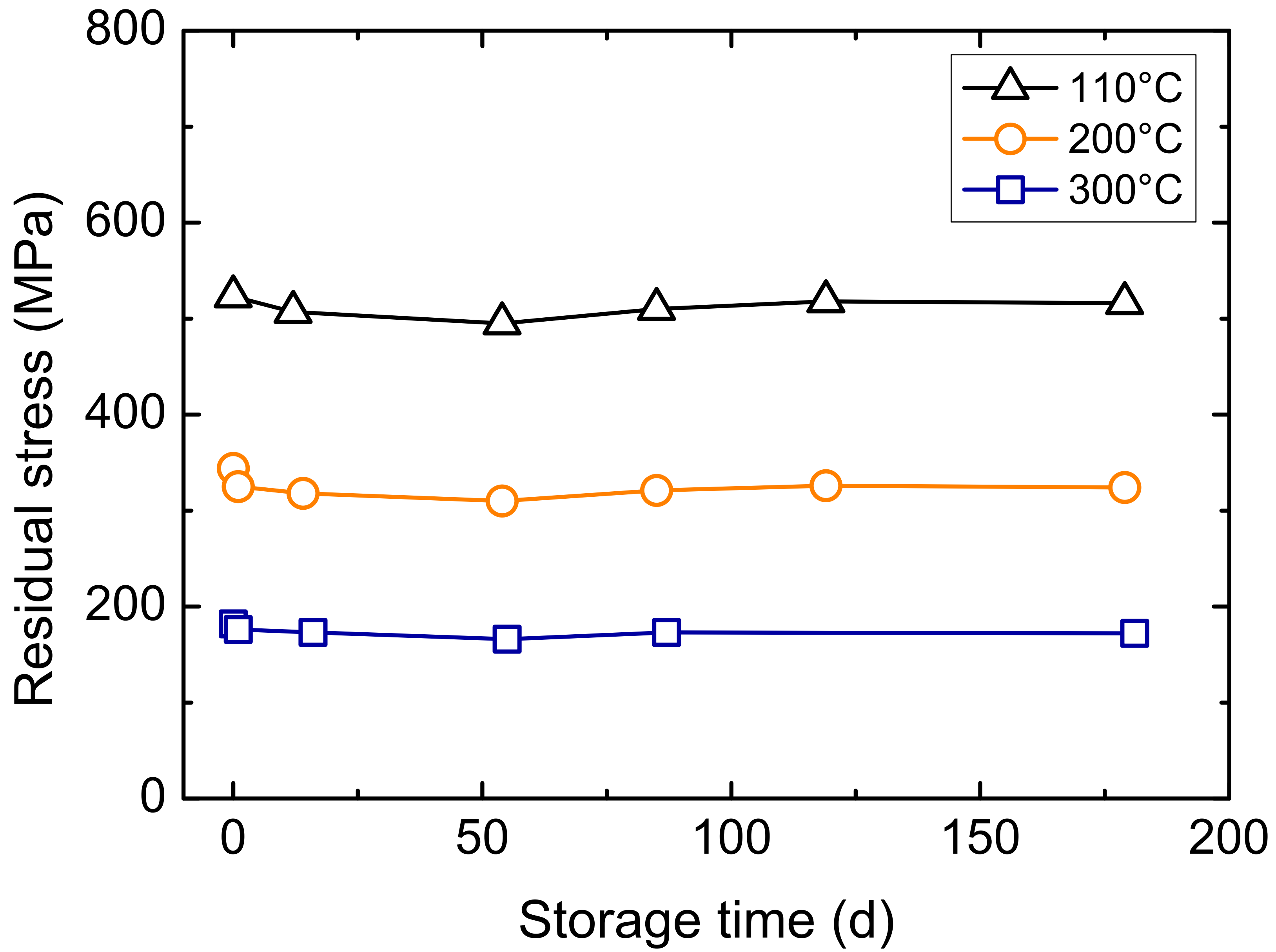

Figure 6A
Click here to download high resolution image

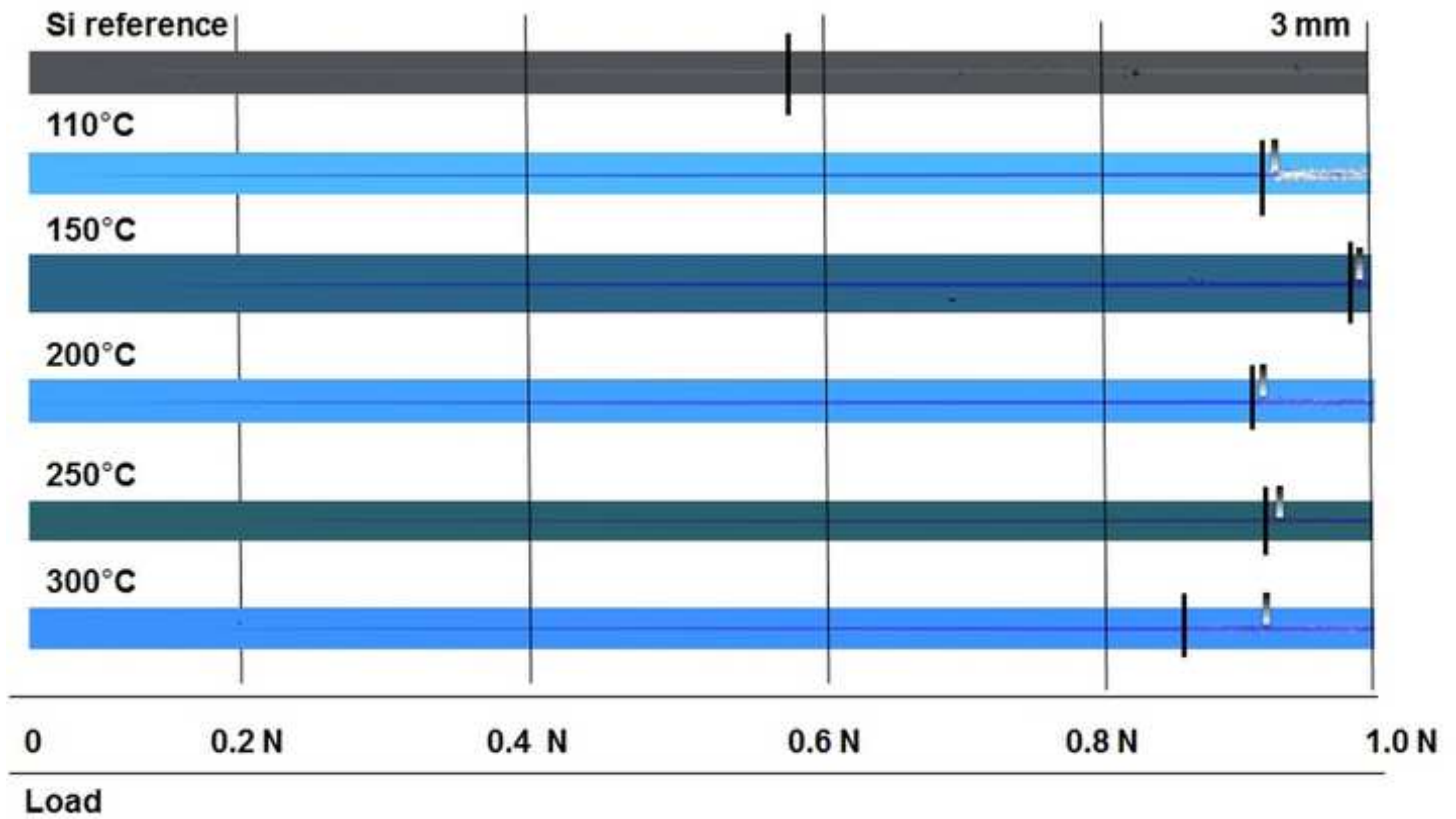

Figure 6B
Click here to download Figures (if any): Figure 6B.eps

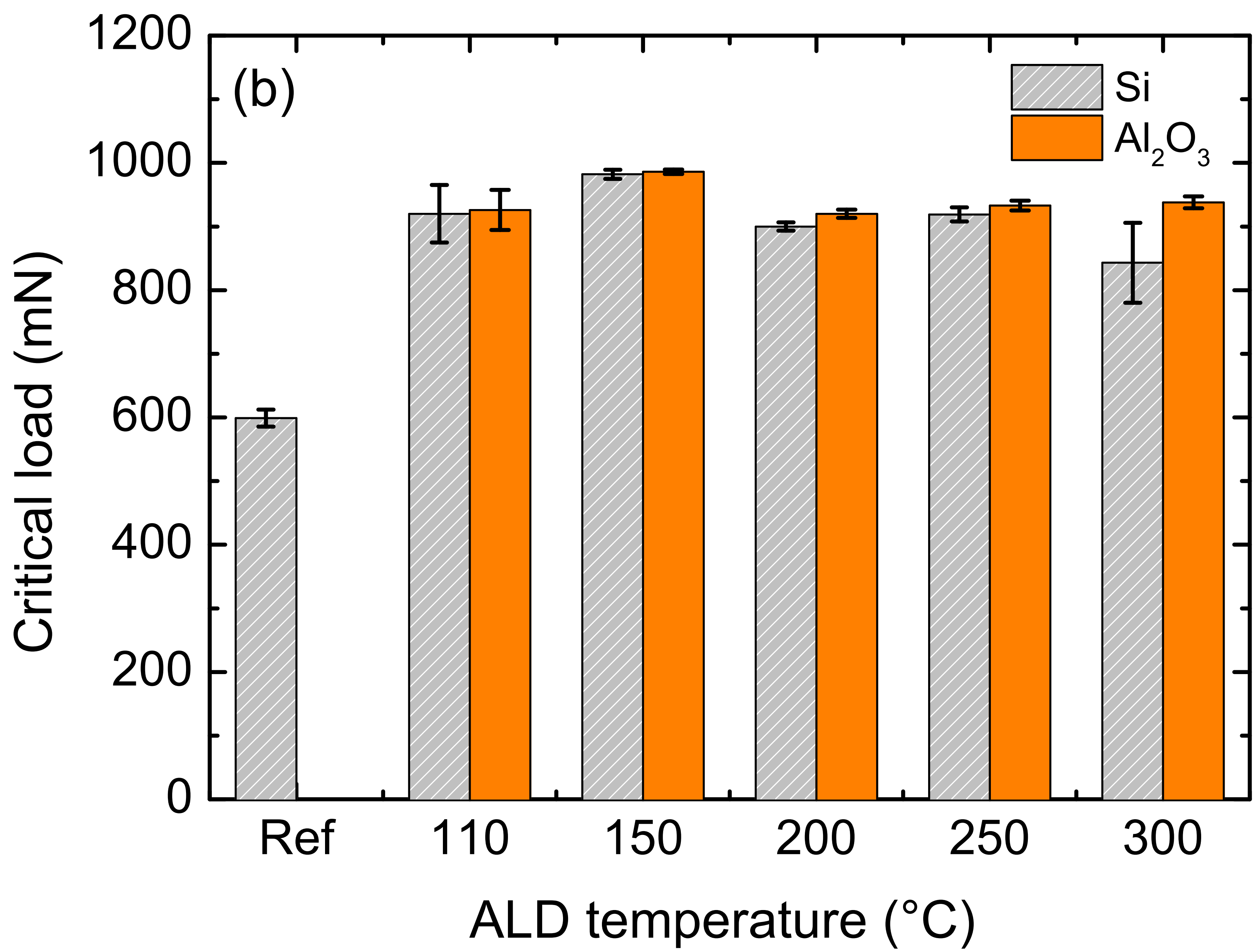

Figure 7
Click here to download high resolution image

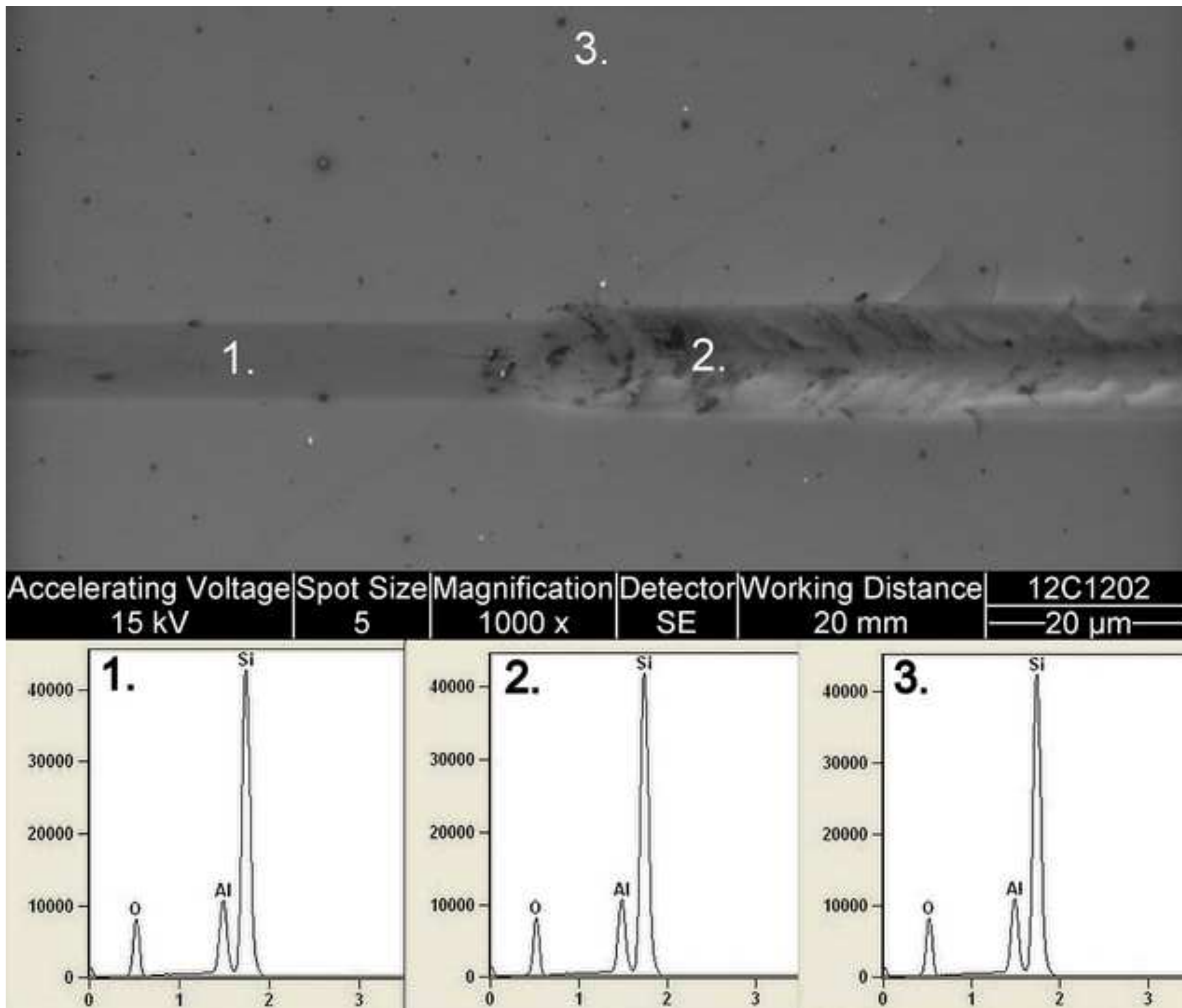

Figure 8
Click here to download high resolution image

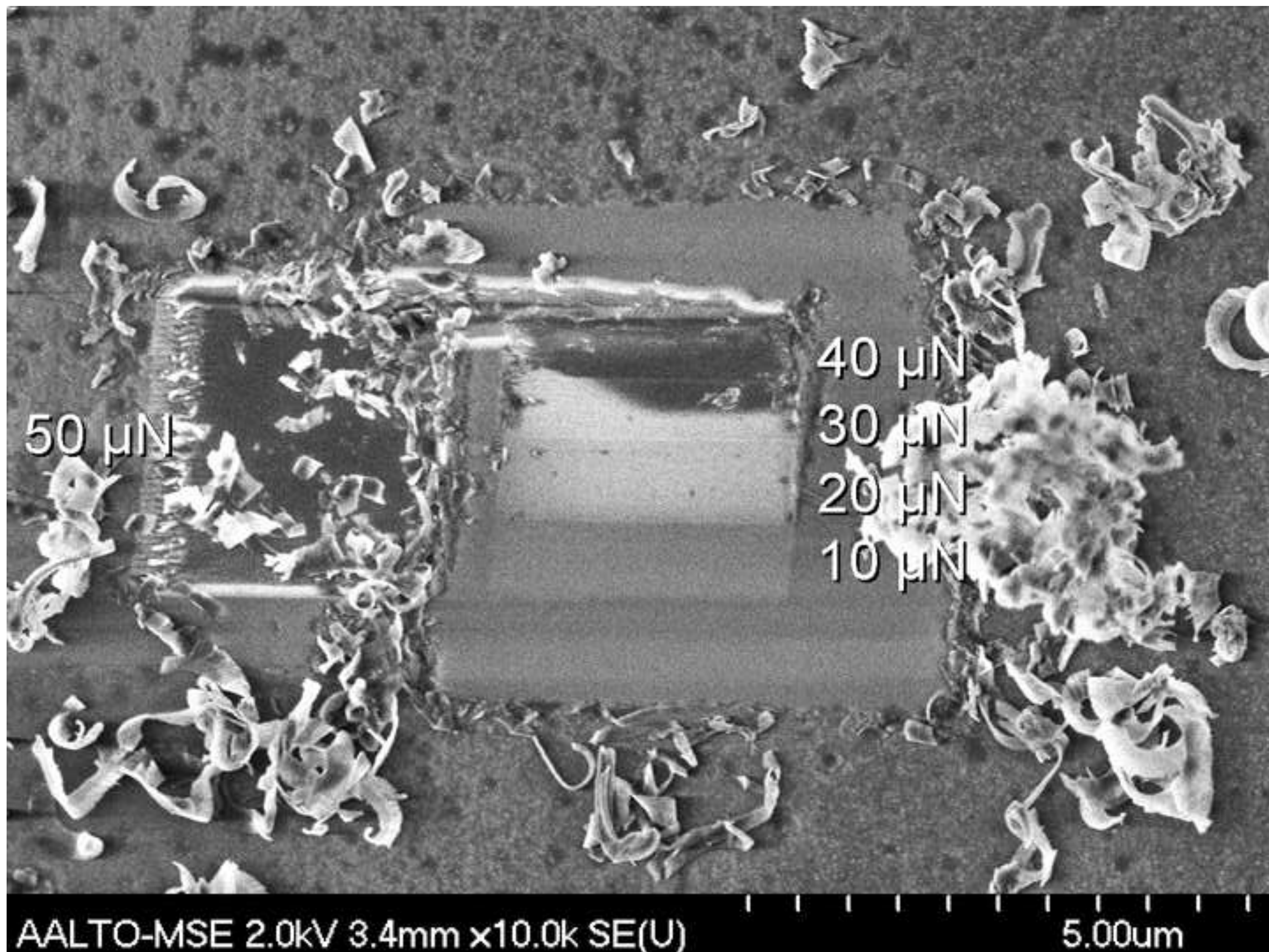

Figure 9

Click here to download Figures (if any): Figure 9.eps

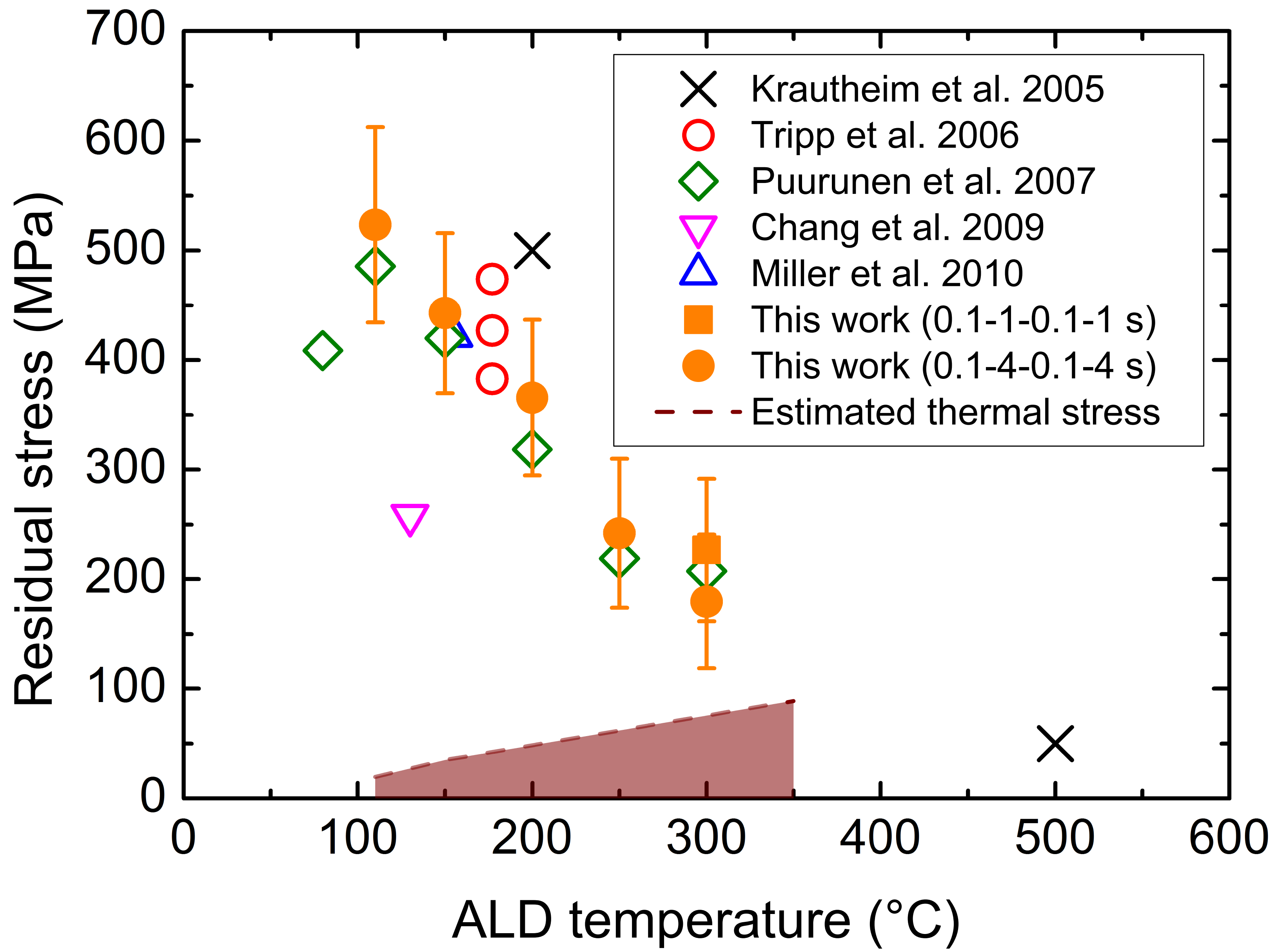

Figure 10A

Click here to download Figures (if any): Figure 10A.eps

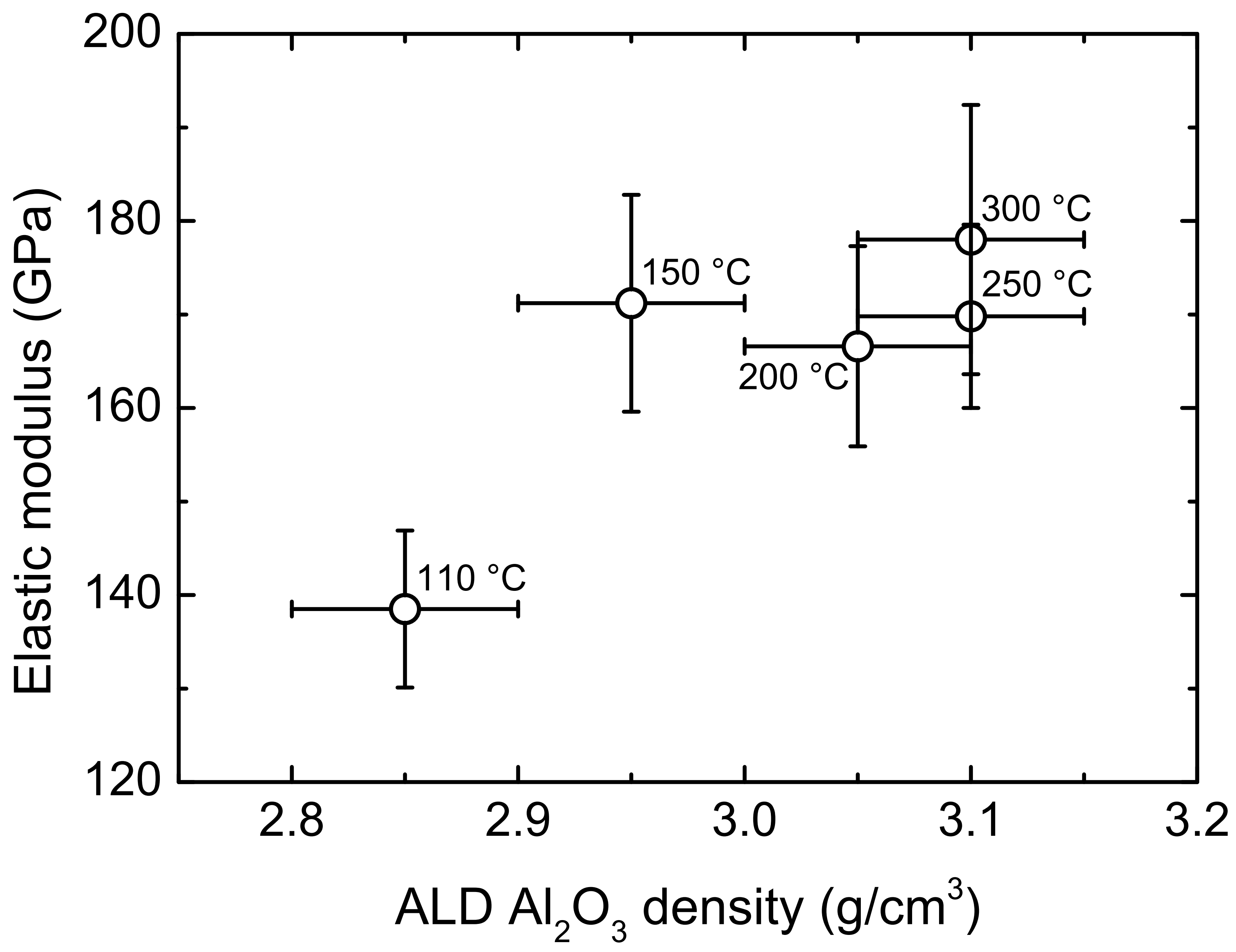

Figure 10B

Click here to download Figures (if any): Figure 10B.eps

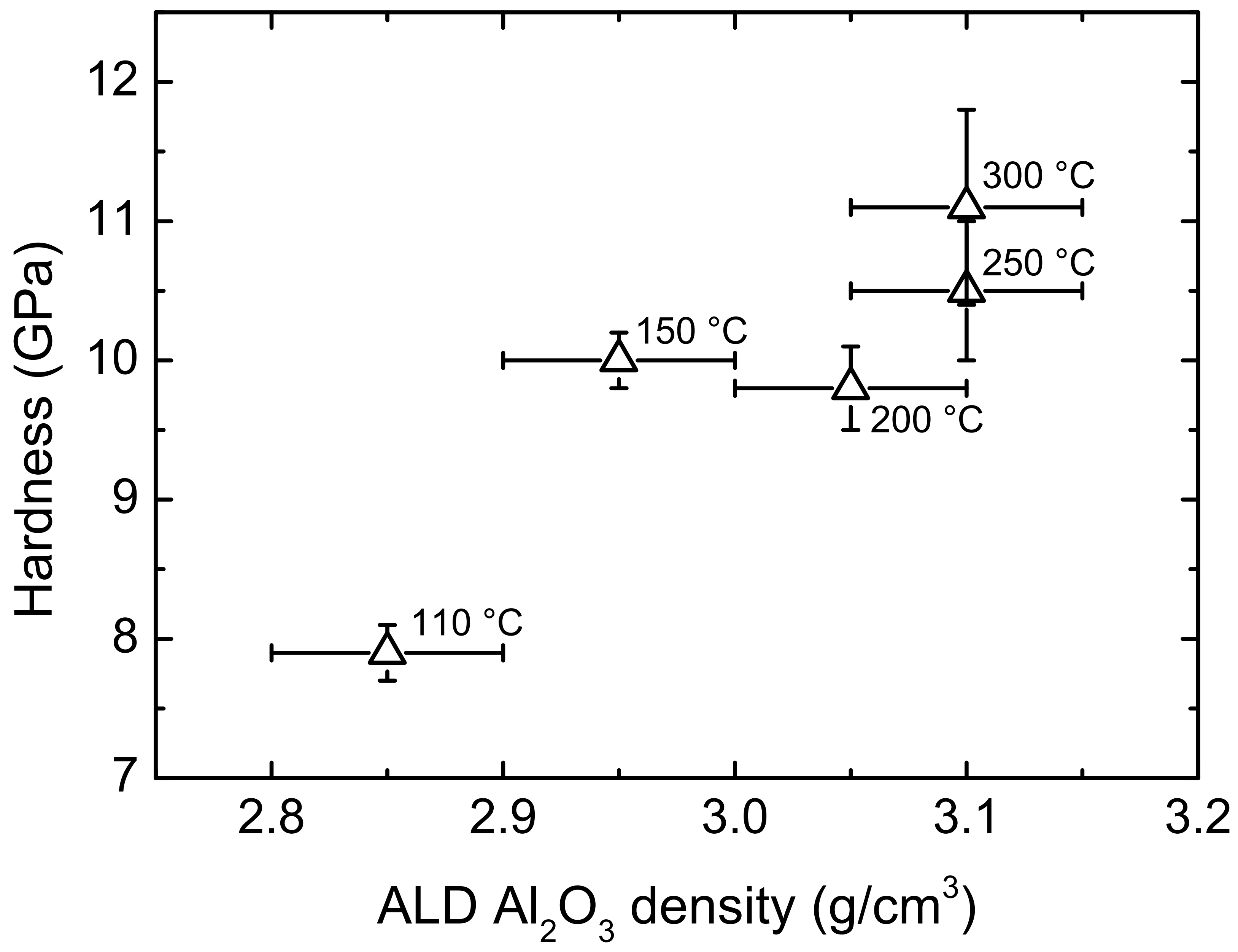

Figure 11

Click here to download Figures (if any): Figure 11.eps

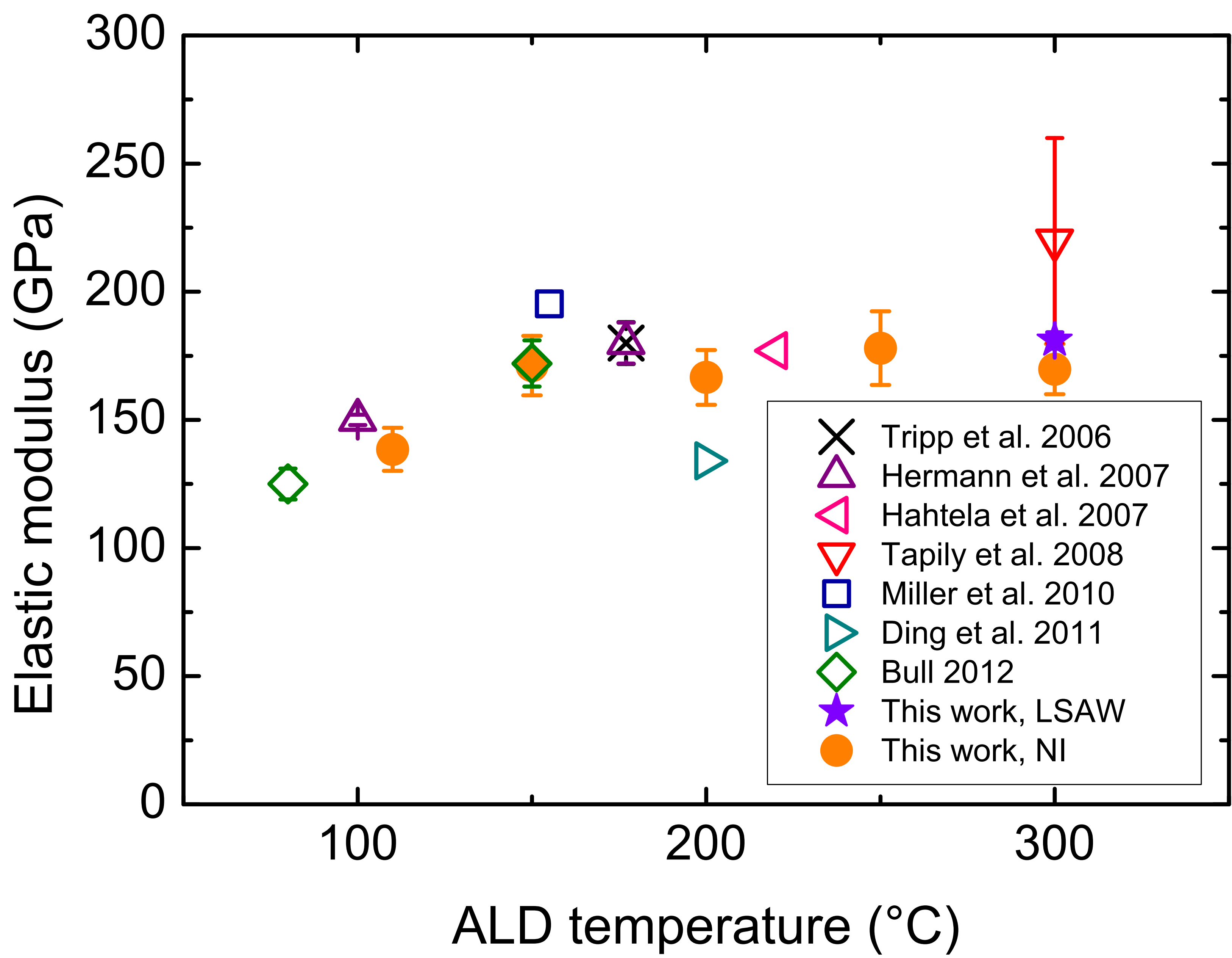

Figure 12

Click here to download Figures (if any): Figure 12.eps